

# Increased Prevalence of Calcium Transients across the Dendritic Arbor during Place Field Formation

## Highlights

- Virtual reality and functional microscopy used to study place field formation
- Local dendritic spikes are likely first events in forming many new place fields
- Release of dendritic inhibition creates plasticity window during novel experiences
- Synaptic plasticity in place cells implicated in forming new place fields

## Authors

Mark E.J. Sheffield, Michael D. Adoff,  
Daniel A. Dombeck

## Correspondence

d-dombeck@northwestern.edu

## In Brief

Sheffield et al. reveal microscopic plasticity-related events occurring in hippocampal neurons that likely underlie spatial memory formation when animals encounter new environments.

# Increased Prevalence of Calcium Transients across the Dendritic Arbor during Place Field Formation

Mark E.J. Sheffield,<sup>1,2</sup> Michael D. Adoff,<sup>1</sup> and Daniel A. Dombeck<sup>1,3,\*</sup>

<sup>1</sup>Department of Neurobiology, Northwestern University, Evanston, IL 60208, USA

<sup>2</sup>Present Address: Department of Neurobiology, Grossman Institute for Neuroscience, The University of Chicago, Chicago, IL 60637, USA

<sup>3</sup>Lead Contact

\*Correspondence: d-dombeck@northwestern.edu

<https://doi.org/10.1016/j.neuron.2017.09.029>

## SUMMARY

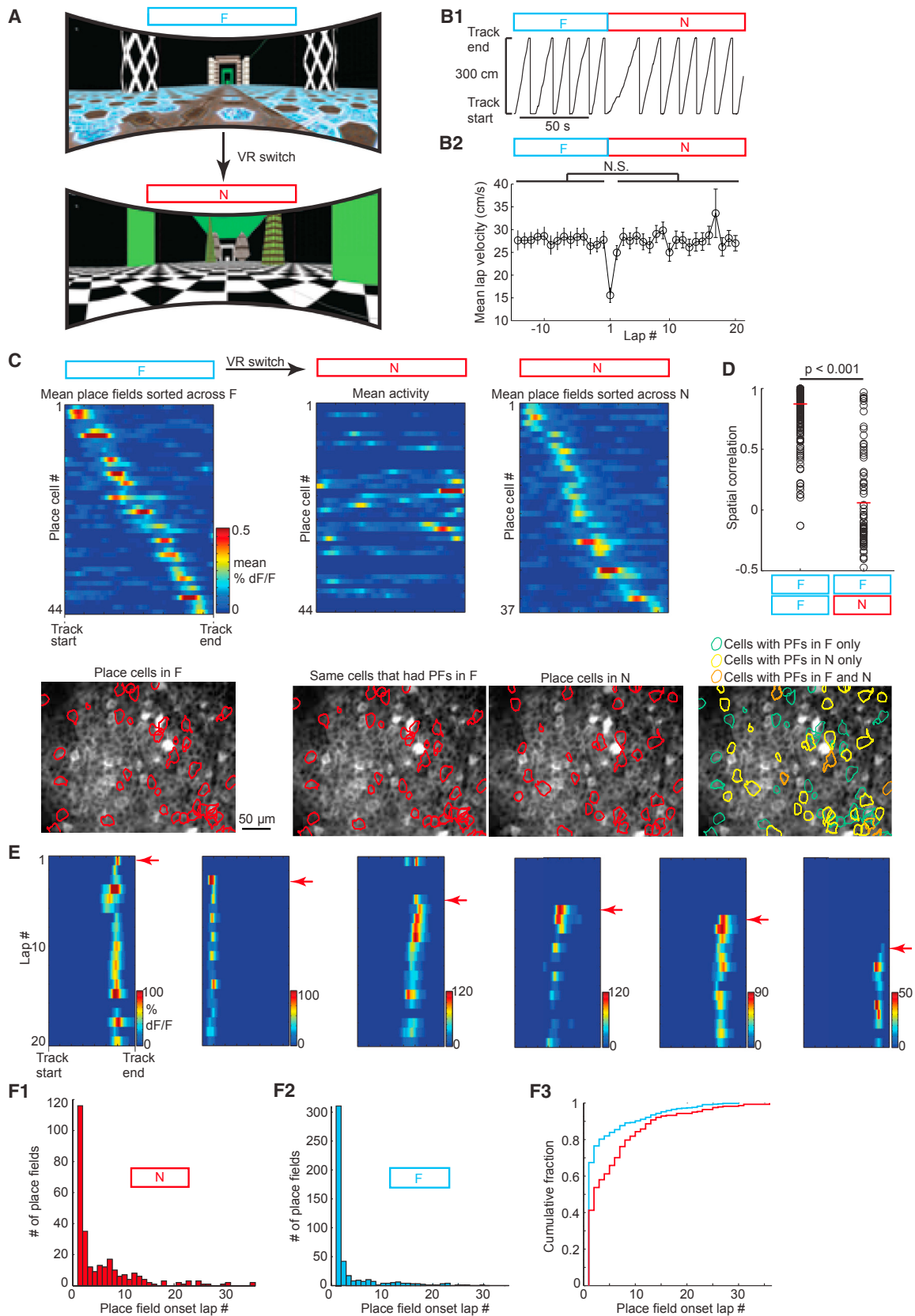
Hippocampal place cell ensembles form a cognitive map of space during exposure to novel environments. However, surprisingly little evidence exists to support the idea that synaptic plasticity in place cells is involved in forming new place fields. Here we used high-resolution functional imaging to determine the signaling patterns in CA1 soma, dendrites, and axons associated with place field formation when mice are exposed to novel virtual environments. We found that putative local dendritic spikes often occur prior to somatic place field firing. Subsequently, the first occurrence of somatic place field firing was associated with widespread regenerative dendritic events, which decreased in prevalence with increased novel environment experience. This transient increase in regenerative events was likely facilitated by a reduction in dendritic inhibition. Since regenerative dendritic events can provide the depolarization necessary for Hebbian potentiation, these results suggest that activity-dependent synaptic plasticity underlies the formation of many CA1 place fields.

## INTRODUCTION

The hippocampus is critical for the formation and storage of spatial memories (Morris et al., 1982; Teng and Squire, 1999). Hippocampal place cells not only fire when animals move through a particular location (place field) (O'Keefe and Burgess, 1971), but during sleep and rest subsequent to the experience they can reactivate in the same (or reverse) sequence as during the experience (Carr et al., 2011; Foster and Wilson, 2006; Sadowski et al., 2016; van de Ven et al., 2016; Wilson and McNaughton, 1994). This has led to the idea that place cell ensembles represent a cognitive map of space and a memory of places. Hippocampal pyramidal neurons, which are the cells that form place fields during spatial navigation, are capable of engaging activity-dependent Hebbian synaptic plasticity

(Bliss and Collingridge, 1993), a potential mechanism by which spatial information can be encoded and stored. Indeed, disruption of components of the molecular pathways involved in synaptic plasticity, such as NMDA receptors or CaMKII, is correlated with behavioral deficits in memory or spatial navigation tasks (Morris et al., 1986; Silva et al., 1992; Tsien et al., 1996). Given that ensembles of place fields are thought to represent spatial memories and are likely used for spatial navigation, these findings have led to the hypothesis that place fields may form *de novo* through activity-dependent synaptic plasticity (Takeuchi et al., 2013), with some evidence supporting this view (Bittner et al., 2015; Monaco et al., 2014). However, there is significant evidence supporting an alternative view, that synaptic plasticity may not be required for place field formation (Cacucci et al., 2007; Dragoi and Tonegawa, 2011, 2013a; Frank et al., 2004; Hill, 1978; Kentros et al., 1998; McHugh et al., 1996). For example, after hippocampal synaptic plasticity is perturbed or blocked, place fields are typically less precise (Cacucci et al., 2007; Kentros et al., 1998; McHugh et al., 1996; Rotenberg et al., 1996), less stable (Kentros et al., 1998; Rotenberg et al., 1996), and fail to shift backward (Ekstrom et al., 2001), but nonetheless place fields still form. Additionally, many place fields are immediately present upon the animal's first traversal across a novel environment (Frank et al., 2004; Hill, 1978). Such a rapidly appearing cognitive map suggests that hippocampal representations could arise through the novel stimulus-dependent selection of pre-strengthened neuronal ensembles (Deguchi et al., 2011; Dragoi and Tonegawa, 2011, 2013a, 2013b; Lee et al., 2012). These results call into question the idea that place fields form *de novo* through synaptic plasticity during experience of a novel environment.

It has been difficult to assess directly the involvement of synaptic plasticity in awake animals engaged in navigation tasks. One step toward this goal would be to investigate dendritic regenerative events (back propagating action potentials or dendritically generated spikes, here collectively referred to as branch spikes [Sheffield and Dombeck, 2015]), which are thought to provide the post-synaptic depolarization necessary for Hebbian potentiation when paired with presynaptic input (Golding et al., 2002; Magee and Johnston, 1997; Schiller et al., 1998). Measuring the occurrence of branch spikes during place field formation would therefore indicate periods in which Hebbian synaptic potentiation could be occurring. A recent



(legend on next page)

study used somatically recorded plateau potentials to infer the existence of branch spiking events throughout the arbor and found that such events may underlie the formation of both artificially induced and spontaneously appearing place fields in familiar environments (Bittner et al., 2015). The technology now exists to record branch spiking directly in behaving mice and, in fact, these events have recently been detected in hippocampal place cells, though again these observations were made during navigation in familiar environments (Sheffield and Dombeck, 2015). This previous research (Sheffield and Dombeck, 2015) demonstrated that branch spiking and somatic firing are often dissociated in place cells, meaning that somatic firing does not provide a direct read out of branch spiking across the arbor. Thus, while there is now evidence to support the idea that branch spiking occurs in place cells and is likely capable of inducing plasticity that can lead to place field firing in familiar environments, it remains unclear whether branch spiking events occur during, or lead to, natural place field formation in novel environments.

Here we used virtual reality (VR) combined with two-photon functional imaging to monitor large populations of hippocampal CA1 neuron somata, co-record CA1 neuron dendrites and somata, or record CA1 interneuron axons while mice were rapidly exposed to novel virtual environments. Global remapping occurred during this paradigm and was similar to that described in real-world environments (Bostock et al., 1991; Fyhn et al., 2007; Leutgeb et al., 2004, 2005; Muller and Kubie, 1987), allowing us to continuously monitor the remapping process from the first moments of novel environment exposure. We found that regenerative dendritic events occur during the first appearance of somatic place field firing and during the first several novel environment traversals the prevalence of these events was increased across the arbor compared to familiar environments or later traversals in the novel environment. For some place fields, localized regenerative dendritic events preceded the appearance of detectable somatic place field firing and predicted the location of the later forming somatic place field. Additionally, we found a transient reduction in the magnitude of calcium transients in the axons of dendrite targeting interneurons on the first few laps in novel environments, while a brief increase in the magnitude of calcium transients in the axons of somatic targeting interneurons was found during a similar period. Finally, we found that when functional NMDA receptors are knocked out in CA1 neurons, the number of place fields that form across the

population is reduced by ~50%. These results suggest that exposure to a novel environment is accompanied by a short time window of reduced dendritic inhibition in CA1, which leads to increased branch spiking, which may potentiate synapses in a subset of neurons to form new place fields. Together these results support the idea that hippocampal activity-dependent synaptic plasticity underlies the formation of a subset of CA1 place fields in the hippocampus during novel environment exposure.

## RESULTS

### Novel Virtual Environment Exposure Leads to Global Remapping in the Hippocampus in Head Restrained Mice

We used VR to implement an environment switch paradigm to induce hippocampal global remapping in head-restrained mice (Figure 1, Figure S1). Mice were trained once a day for 7 days on a 1D treadmill to traverse a 3 m virtual visual linear track (Figure 1A, Figures S1A and S1B) for water rewards (Heys et al., 2014). Subsequently, on experimental day 1, mice traversed this familiar environment (F) for at least 15 laps before F was rapidly (~30 ms) switched to a novel environment (N; Figure 1A, Figures S1A and S1B). Mice then experienced N for at least 20 laps, before being placed back in their home cage. The following day (experimental day 2) the mice were re-exposed to N where they traversed the track for at least 20 laps. An F-to-N switch was implemented twice for each mouse, with different environments for each switch (Figures S1A and S1B). To quantify behavior before, during, and after the switch, we measured mean lap velocity (Figure 1B2), stopping probability (Figure S1D) and mean stopping time (Figure S1E) on each lap. We found that the first lap in N was traversed slower ( $15.6 \pm 1.5 \text{ cm}^{-\text{s}}$  SEM on first lap in N versus  $27.7 \pm 0.5 \text{ cm}^{-\text{s}}$  SEM in F,  $p < 0.001$ , paired t test,  $n = 32$  sessions,  $n = 16$  mice) and with more stops ( $0.8 \pm 0.1$  SEM on first lap in N versus  $0.19 \pm 0.02$  SEM in F,  $p < 0.01$ ) that lasted longer ( $5.4 \pm 2.1 \text{ s}$  SEM on first lap in N versus  $0.63 \pm 0.13 \text{ s}$  SEM in F,  $p < 0.001$ ) compared to F, but behavior quickly stabilized such that on all subsequent laps in N, mean lap velocity and mean stopping time were not different compared to F (mean lap velocity from all laps and excluding lap 1 in N:  $27.7 \pm 0.5 \text{ cm}^{-\text{s}}$  in F versus  $27.7 \pm 0.5 \text{ cm}^{-\text{s}}$  in N,  $p > 0.05$ , paired t test; mean lap stopping time from all laps following lap 1:  $0.63 \pm 0.13 \text{ s}$  SEM in F versus  $1.04 \pm 0.25 \text{ s}$  SEM in N,  $p > 0.05$ ), and mean stopping probability was only slightly increased (mean lap stopping

**Figure 1. Switching Virtual Environments Causes Global Remapping**

- (A) Examples of familiar (F) and novel (N) virtual environments.
- (B1) Single mouse behavior showing track position versus time over F to N switch.
- (B2) Summary across all mice of mean lap velocity over F to N switch ( $n = 16$  mice;  $n = 32$  F to N switches). Mean  $\pm$  SEM; N.S. Paired t test,  $p > 0.05$ .
- (C) Bottom left: CA1 field of view indicating place cells encoding F (red). Top left: mean place fields from cells (red) sorted by track position. Bottom middle: same field of view and cells as in bottom left. Top middle: mean activity of indicated cells in N sorted in same order as top left. Bottom right: same field of view as bottom left with all place cells encoding N (red). Top right: mean place fields from cells (red) sorted by track position. Bottom far right: same field of view as bottom left with all place cells colored to indicate F, N, or both encoding.
- (D) Place field spatial correlation within F versus across F to N.  $p < 0.001$ , unpaired t test.
- (E) Somatic place field transients shown lap by lap in N for 6 example cells; first row represents first traversal mouse ever made across N. Red arrows indicate place field onset lap.
- (F1 and F2) Histograms of place field onset lap number from all mice in N (F1;  $n = 4$  mice;  $n = 8$  sessions in N) and F (F2;  $n = 3$  mice;  $n = 8$  session in F).
- (F3) Cumulative fraction plots of the data in F1 and F2. Place field onset lap distribution was shifted (Wilcoxon rank sum test,  $p < 0.001$ ) such that place fields appeared earlier in F versus N.

probability from all laps following lap 1:  $0.19 \pm 0.02$  in F versus  $0.30 \pm 0.02$  SEM in N,  $p < 0.001$ , paired t test). Therefore, our VR paradigm allows for rapid switching from familiar to novel environments with relatively little change in behavior after the first traversal.

We then asked whether the switch from F to N caused global remapping in the hippocampus, a phenomenon that occurs in the real world when animals are placed in novel environments (Bostock et al., 1991; Fyhn et al., 2007; Leutgeb et al., 2004, 2005; Muller and Kubie, 1987). We used our previously described methods to optically record somatic calcium transients (a measure of action potential firing; GCaMP6f) in populations of CA1 pyramidal neurons and defined the place firing field(s) of neurons within the population (Dombeck et al., 2010; Sheffield and Dombeck, 2015). Over all traversals in F, we found all neurons with significant mean place fields. From eight sessions in F ( $n = 4$  mice), we identified 347 place cells. Some place cells expressed two place fields, and we treated each place field independently (382 place fields total). A typical CA1 field of view contained place cells (Figure 1C, bottom left) expressing place fields tiling the track (Figure 1C, top left). We then switched from F to N and measured the firing patterns of the same neurons (the place cells that had place fields in F; Figure 1C, bottom middle) over all traversals in N on experimental day 1 (Figure 1C, top middle). We found that, across all mice, many cells identified as having place fields in F did not have place fields in N (301/382 place fields). For the cells that did have place fields in both F and N, the location of the fields were not correlated (see STAR Methods, Figure S1F) and showed significantly less spatial correlation compared to fields examined within F (Figure 1D, spatial correlation within first half to second half of F =  $0.87 \pm 0.01$  SEM,  $n = 382$  place fields versus across F to N =  $0.06 \pm 0.04$  SEM,  $n = 81$  place fields,  $p < 0.001$ , unpaired t test). However, additional place cells appeared in N ( $n = 263$  total place cells;  $n = 279$  total place fields across all mice; Figure 1C, bottom right) and their place fields tiled the novel track (Figure 1C, top right). These data are consistent with global remapping in real-world environments (Bostock et al., 1991; Fyhn et al., 2007; Leutgeb et al., 2004, 2005; Muller and Kubie, 1987) and in VR in body-tethered rats (Aronov and Tank, 2014) and indicate that global remapping occurs in the hippocampus of head-restrained mice following a rapid switch from a familiar to a novel VR environment.

Next we tracked somatic calcium transients of the place fields that appeared in N on each lap starting from the very first lap in N (Figure 1E). We noticed that place fields abruptly appeared on a range of laps during the initial exposure to N (Figure 1E), an observation also consistent with remapping in real-world novel environments (Frank et al., 2004; Hill, 1978). To quantify this, for each place field detected in N, we identified the lap in which transients first began to robustly occur within the place field (place field onset lap; Figure 1E, red arrows; see STAR Methods). Pooling the place fields from all mice ( $n = 4$  mice,  $n = 8$  sessions in N), we found that 116/279 place fields appeared on the first lap in N, 35/279 had a place field onset lap of 2, and 128/279 had a place field onset lap greater than lap 2 (Figure 1F1; a different distribution compared to the same measurements in F, see Figures 1F2 and 1F3). Overall, the vast majority of place fields appeared within the first several laps of N (224/279 (80%) within 8

laps and 261/279 (94%) within 16 laps;  $92.3 \pm 2.4$  s SEM and  $179.5 \pm 3.2$  s SEM was required to complete 8 and 16 laps respectively). These results demonstrate that exposure to novel environments leads to the appearance of place fields over the first few traversals and minutes.

### Prevalence of Dendritic Branch Spikes Is Increased in Place Cells during Initial Exposure to Novel Environments and Predicts Final Place Field Location

To test whether synaptic plasticity could occur during the initial exposure to N, when the majority of place fields first appear, we asked whether branch spiking (Sheffield and Dombeck, 2015), which can provide the post-synaptic depolarization necessary for Hebbian synaptic potentiation (Golding et al., 2002; Magee and Johnston, 1997; Schiller et al., 1998), occurred or varied during this period. We sparsely labeled CA1 neurons with GCaMP6f (Figure 2A) and used multi-plane two-photon imaging to co-acquire time series datasets from CA1 basal dendrites and their parent somata ( $n = 9$  mice,  $n = 18$  sessions in N;  $n = 13$  place cells;  $n = 17$  place fields; number of dendrites imaged per cell: range = 9–36, mean =  $17 \pm 2$ ; distance of dendritic imaging plane from somatic imaging plane: range =  $61\text{--}103$   $\mu\text{m}$ , mean =  $83 \pm 8$   $\mu\text{m}$  [distal tips located in a plane  $\sim 120$   $\mu\text{m}$  from somata]) (Sheffield and Dombeck, 2015). Individual dendrites were assigned to their parent somata offline using dendrite tracing from a z series image stack (Sheffield and Dombeck, 2015; STAR Methods). To quantify the prevalence of branch spiking over traversals in N, we calculated the branch spike prevalence (BSP) as the fraction of recorded branches from each cell with branch spikes during each traversal across the place field when somatic firing was detected (Figure 2B) (Sheffield and Dombeck, 2015). We first observed that branch spiking was always associated with place field formation: branch spiking in the basal dendrites always occurred and was typically widespread during the first detectable somatic firing events in the place field ( $n = 17$  place fields with branch spikes, mean BSP =  $0.80 \pm 0.07$  SEM, range: 0.20–1.00 during first somatic firing in field;  $n = 11$  place fields with BSP > 0.96 and  $n = 4$  with BSP < 0.45; Figures 2A and 2B). During this first traversal and the following traversals across the place field in which somatic firing was detected, we observed variations in BSP from traversal to traversal (Figures 2A and 2B). For individual place cells, we noticed that the average BSP (binned over 4 laps) was nearly always elevated when the somatic place field first appeared during the initial exposure to N and decreased with lap number during the session (Figure 2B, right). This effect was significant on average across all place cells from all mice exposed to N (Figure 2C) and importantly did not occur at the beginning of sessions when mice were first exposed to F (Figures S2I and S2J). We measured average BSP from place cells in F (mean BSP =  $0.43 \pm 0.03$  SEM), which was significantly lower than the average BSP that occurred during laps 1–4 in N (mean BSP =  $0.75 \pm 0.08$  SEM,  $p < 0.01$ , unpaired t test), laps 5–8 in N (mean BSP =  $0.65 \pm 0.07$  SEM,  $p < 0.05$ , unpaired t test; Figure 2C) and the first 4 laps from place field onset (mean BSP =  $0.66 \pm 0.05$  SEM,  $p < 0.01$ , unpaired t test; Figure 2F). We also compared average BSP during the first 8 (Figure 2D) or 16 laps (Figure 2E) in N to later laps in N (>lap 16) in

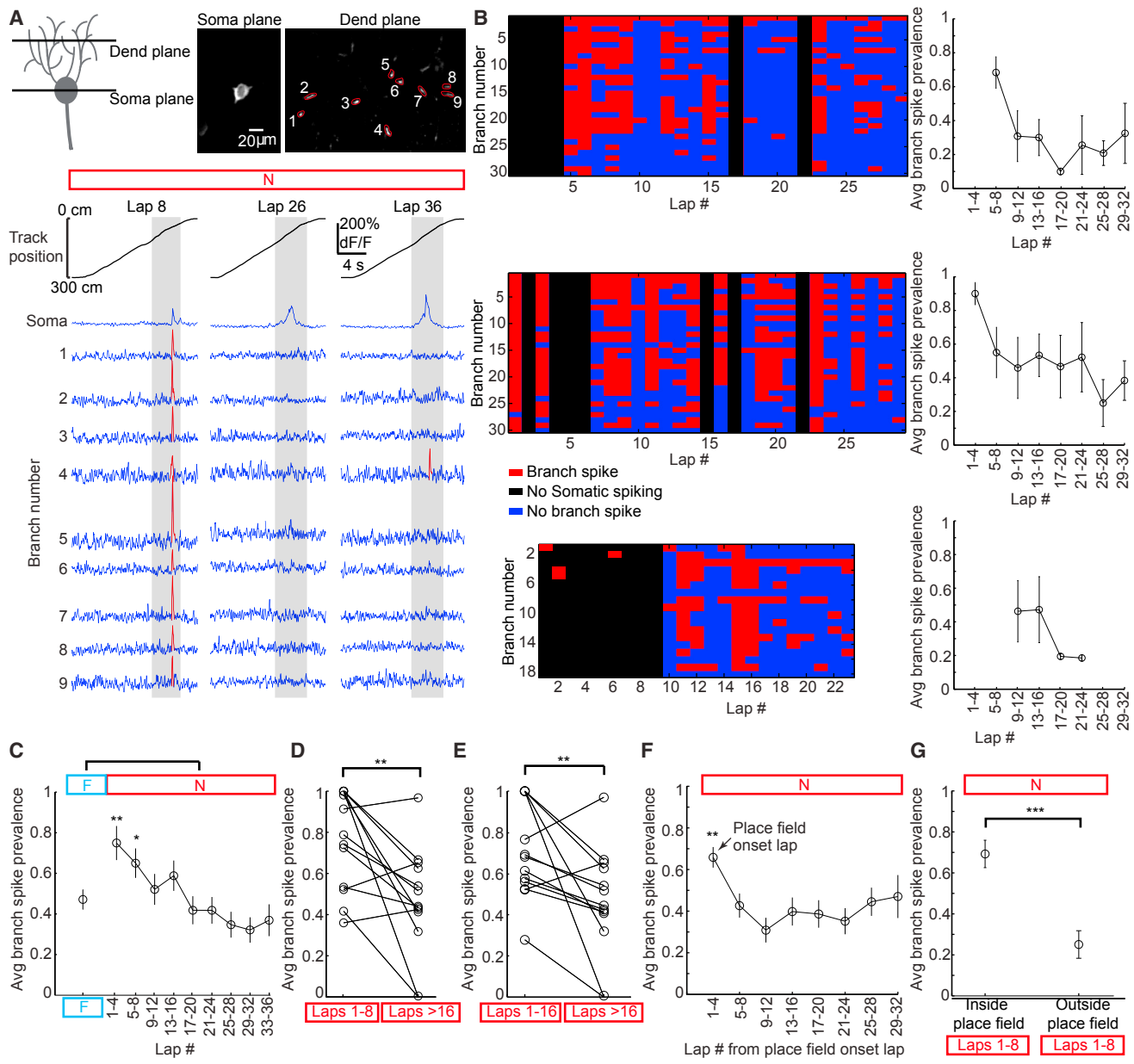


**Figure 2. Dendritic Branch Spikes Are More Prevalent during Initial Exposure to Novel Environments and Predict Future Place Field Location**

(A) Top: cartoon depicting two-photon imaging planes in the soma and basal dendrites of pyramidal cells and co-acquired images of place cell soma and dendrites from the same cell. Bottom:  $\Delta F/F$  traces from the (co-acquired) soma and numbered dendritic branches during three place field traversals (gray columns, mean place field over session in N) in N. Red traces, transients of  $p < 0.001$  from bootstrapping.

(B) Colored plots (left; three different place cells from two mice) show occurrence of detectable branch spiking in each imaged branch (rows) in the somatic place field on each lap in N, each column represents a different lap in N; first column represents first traversal mouse ever made across N. Red, significant transient in the imaged branch; blue, no significant transient in the branch during a co-occurring somatic calcium transient; black, no significant transient in the branch or soma. Right, plots of mean BSP (4 laps binned) versus laps in N from example cells on left. Error bars indicate SEM.

(C) Summary across all mice of mean BSP in F ( $n = 10$  place fields,  $n = 5$  mice) and N (4 laps binned;  $n = 18$  place fields,  $n = 9$  mice). Error bars indicate SEM.

(D) Mean BSP from first 8 laps versus all laps following lap 16 in N ( $n = 13$  place fields,  $n = 7$  mice). \*\*, paired t test,  $p < 0.01$ .

(E) Same as (D) but using first 16 laps. \*\*, paired t test,  $p < 0.01$ .

(F) Same as (C) but aligned to place field onset lap for each cell (depicted as lap 1). Error bars indicate SEM.

(G) Average BSP in place fields versus outside of place fields in first 8 laps of N. Error bars indicate SEM. \*\*\*, paired t test,  $p < 0.001$ .

the same cells and found average BSP was significantly higher early versus late in both cases (mean BSP from all laps following lap 16 =  $0.38 \pm 0.04$  SEM versus laps 1–8 =  $0.69 \pm 0.05$  SEM,  $p < 0.01$ , paired t test, and versus laps 1–16 =  $0.62 \pm 0.04$  SEM,  $p < 0.01$  paired t test). Again, these changes in BSP as a function of lap number were not seen in F (Figure S2 J).

Since dendritic branch spiking and somatic firing can be dissociated in CA1 place cells (Sheffield and Dombeck, 2015), we next asked whether the location of branch spiking on the track during initial exposure to N was an indicator of where the mean place field would be located at the end of the session. We determined the track location of the mean somatic place field calculated from laps in the last half of the session in N. We then measured the average BSP that occurred within this location and compared it to the average BSP outside this location (fraction of branches with branch spikes during somatic firing detected outside of place field) during the first eight laps of the session in N. We found that average BSP in the first eight laps was significantly higher within the final place field location versus outside of this location, predicting the final field location (Figure 2G, average BSP inside =  $0.67 \pm 0.07$  SEM, outside =  $0.25 \pm 0.07$  SEM, paired t test,  $p < 0.001$ ). Together, the above findings demonstrate that branch spiking in basal dendrites is elevated during somatic place field firing in the first several traversals of a novel environment and is most prevalent at the track location of the final place field. These results support the idea that CA1 synaptic plasticity is taking place during a window in which place fields first appear in novel environments.

### Dendrite-Localized Calcium Transients Predict the Track Location of Subsequent Delayed Onset Place Fields

As described above (Figures 1E and 1F1), some place cells in N had a delay period before their place fields first appeared. If synaptic plasticity is occurring in these cells during this delay period to contribute to the formation of new place fields, it appears to occur in the absence of somatic action potential firing and back-propagation into the dendrites. We therefore looked for dendrite-localized calcium transients that might result from local clustered synaptic input (possibly generating local regenerative events) capable of inducing synaptic potentiation in the absence of somatic firing (Brandalise et al., 2016; Losonczy and Magee, 2006; Major et al., 2008; Milojkovic et al., 2007; Oakley et al., 2001; Palmer et al., 2014; Schiller et al., 2000; Weber et al., 2016; Wei et al., 2001).

Across 17 delayed onset place fields in N, we detected 33 calcium transients that occurred in the basal dendrites in the absence of detectable somatic calcium transients (Figure S3B) during the delay period (these occurred across  $n = 8$  place fields from  $n = 7$  mice). Most of these dendrite-localized transients occurred in single branches (24/33; Figure 2B, bottom, Figure 3A) with no detectable transients in the other imaged branches (mean number of branches imaged per cell was 17, range: 9–36). Interestingly, the other 9 dendritic transients occurred simultaneously in 9 different branches of the same cell (12 branches were imaged in total), again without a detectable somatic transient (Figure S3A). The majority (30/33) of these dendrite localized transients appeared to invade an area encom-

passing both shaft and spines across the imaged section of the local branch (Figures 3B and 3C; dendritic area of significant  $\Delta F/F$  increases greater than single spines  $5.58\text{--}26.11 \mu\text{m}^2$ ,  $n = 30$ ) and therefore spread further across the branch than a separate class of calcium transients that were restricted to single spines (dendritic area of significant  $\Delta F/F$  increases in spines  $0.36\text{--}2.51 \mu\text{m}^2$ ,  $n = 63$ , data not shown) (Sheffield and Dombeck, 2015). The spatial spread for the 30 dendrite localized transients represents a lower bound of the actual extent of the transients, since our imaging plane transected only a small region of each branch. We then identified the track locations where these 30 dendrite localized transients occurred and found that 22/30 occurred within the boundaries of the somatic place field that would soon form (occurring  $9.1 \pm 4.6$  laps SD and  $183.2 \pm 96.6$  s SD before place field onset), occurred more frequently at the beginning of these boundaries (19 occurred earlier on the track and 3 occurred later on the track relative to the mean somatic place field center of mass; chi-square test for proportional difference,  $p < 0.001$ ), and occurred more within these boundaries than in other track locations (Figures 3A and 3D; chi-square test for proportional difference,  $p < 0.001$ ).

We next turned to an ex vivo brain slice preparation to investigate possible mechanisms for the generation of dendrite localized calcium transients. We used established glutamate uncaging techniques to mimic synaptic inputs at selected spines along a single basal dendrite of a CA1 neuron expressing GCaMP6f (Bloodgood and Sabatini, 2007; Losonczy and Magee, 2006; Losonczy et al., 2008). Using a two-photon microscope to image dendrites during spine stimulation, we found that simultaneous (within 5 ms) clustered input within  $5\text{--}15 \mu\text{m}$  onto multiple spines (3 or more) often generated dendritic calcium transients that spread beyond the stimulated spines and into the nearby shaft (Figure S3D), a signature suggesting local dendritic spike generation (Brandalise et al., 2016; Losonczy and Magee, 2006; Major et al., 2008; Milojkovic et al., 2007; Oakley et al., 2001; Palmer et al., 2014; Schiller et al., 2000; Weber et al., 2016; Wei et al., 2001). These dendrite-localized calcium transients stimulated in slice had transient amplitudes and durations similar to the dendrite-localized transients recorded during the delay period of delayed onset place fields in behaving mice (Figure S3).

Based on the observations that the 30 dendrite-localized calcium transients (1) occur in the absence of detectable somatic calcium transients, (2) invade an area larger than a single spine and encompass local spines and shaft in the imaging plane, and (3) have amplitudes and durations similar to transients stimulated with clustered synaptic input in slice, we conclude that these dendrite-localized calcium transients are caused by clustered input onto single basal branches, presumably generating local dendritic spikes, during the delay period in delayed onset place cells. Some of these 30 dendrite-localized calcium transients may represent nonlinear amplification of spine calcium signals by clustered synaptic input that does not reach full dendritic spike status (Weber et al., 2016), and therefore we refer to these 30 events as “putative” local dendritic spikes. Importantly, both full dendritic spikes and clustered inputs that just fall short of generating local dendritic spikes are capable of triggering synaptic potentiation (Weber et al., 2016).

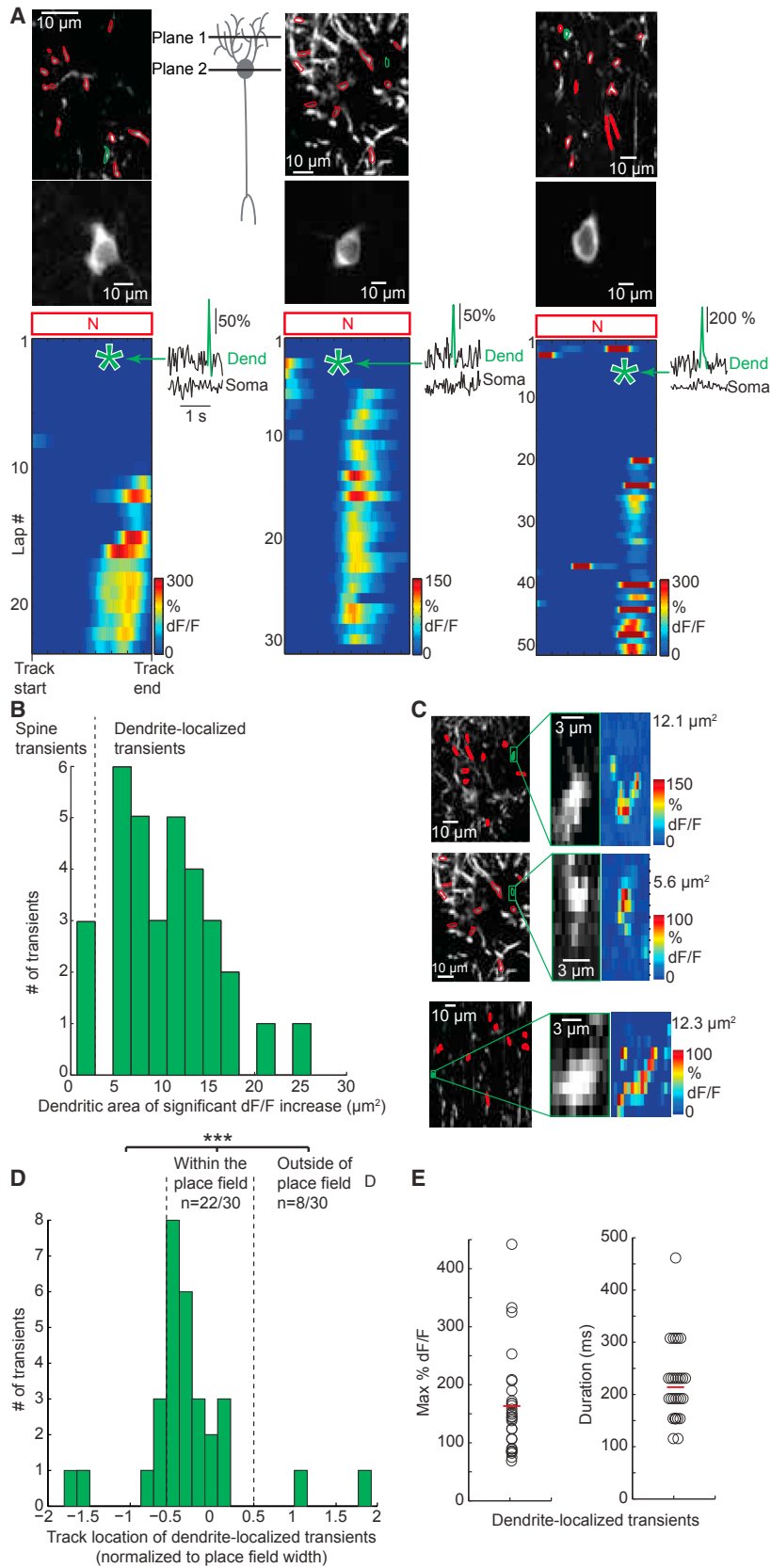


**Figure 3. Putative Local Dendritic Spikes Predict the Location of Delayed Onset Somatic Place Fields**

(A) Cartoon depicts co-recording from soma and basal dendrites of CA1 pyramidal cells. Three example place cells and their dendritic branches are shown (red regions, all branches belonging to the co-imaged soma; green regions, dendrites that displayed a dendrite-localized calcium transient; non-selected dendrites from different cells). Bottom, somatic place field transients lap by lap in N; first row representing first traversal mouse ever made across N. Green stars, track location where dendrite-localized calcium transient detected in indicated branch (at top) in the absence of a detectable somatic calcium transient (time series  $\Delta F/F$  traces from the branch and soma shown at right).

(B) Histogram of the area of significant  $\Delta F/F$  increase for each dendrite-localized calcium transient detected during the delay period of delayed-onset place fields. The area of significant  $\Delta F/F$  increase for known single spine-restricted calcium transients (likely single synaptic inputs, not shown) are all less than the dotted line.

(C) Three example dendrites showing dendrite-localized calcium transients from different place cells during delay period. Left: same as (A, top). Middle: magnified view of the indicated dendrites. Right:  $\Delta F/F$  image of the indicated dendrites during dendrite-localized calcium transients. Area of significant  $\Delta F/F$  increase ( $>3$  SD) at right.

(D) Histogram of track locations of all dendrite-localized calcium transients that occurred during the delay period of delayed-onset place fields relative to the location of the later forming somatic place field (somatic field center at 0; running direction from negative to positive; only transients  $>$  threshold in (B) included). \*\*\*, chi-squared proportionality test,  $p < 0.001$ .

(E) Max  $\Delta F/F$  and transient duration for each dendrite-localized calcium transient (only transients  $>$  threshold in B included).

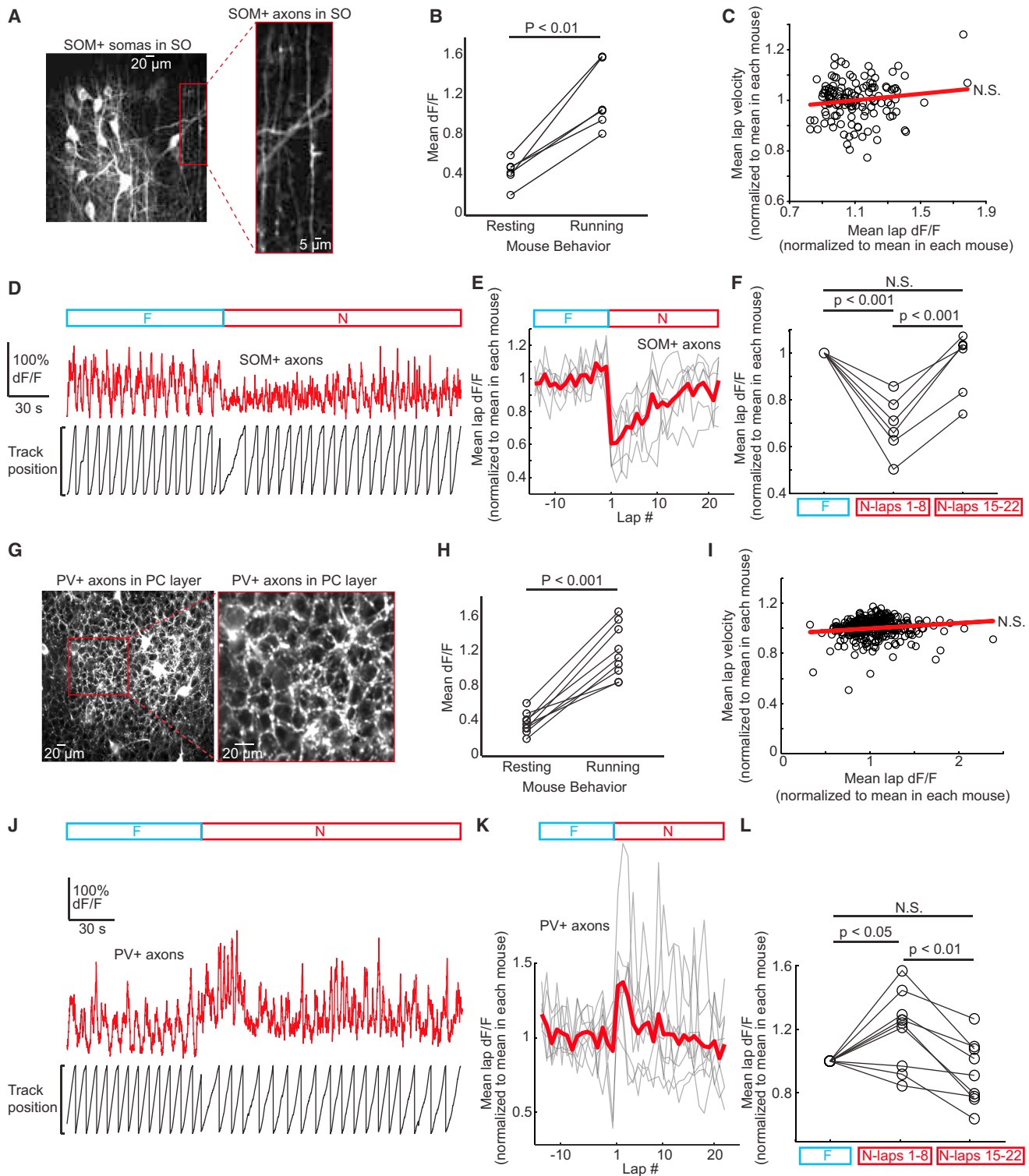


**Figure 4. Dendritic Inhibition Is Transiently Reduced and Somatic Inhibition Is Transiently Increased following Exposure to Novel Environments**

(A) GCaMP6f-expressing SOM+ interneuron cell bodies (left) and axons (right) in stratum oriens of CA1 *in vivo*.

(B) Mean SOM+ interneuron axonal  $\Delta F/F$  (average over all axons in field) during running versus resting in F (paired t test). Open circle, means from six sessions in F from three mice.

(legend continued on next page)

To approximate the frequency of these putative local dendritic spikes across the whole basal dendritic arbor of each delayed forming place cell ( $n = 17$ ) on each lap during the delay period, it was first necessary to estimate the spatial spread of the putative local dendritic spikes *in vivo*. We made a separate set of high-resolution time series movies from long stretches of basal dendritic branches of place cells (not during delay periods,  $n = 3$  mice). We identified four putative local dendritic spikes from three different branches that closely resembled those observed in slice (Figures S3C and S3D). The total length of dendrite invaded by these transients could be measured since they were contained within the imaged branch: range of 5.9–8.5  $\mu\text{m}$ , mean of 7.5  $\mu\text{m}$ , similar to other reports (Brandalise et al., 2016; Lavzin et al., 2012; Major et al., 2008; Palmer et al., 2014; Schiller et al., 2000; Weber et al., 2016). We first assumed that the spread of these 4 putative local dendritic spikes represents an estimate of the spread of the 30 putative local dendritic spikes observed during the delay period (the two classes of putative spikes, 4 and 30, had similar amplitude and kinetics as well). Then, based on this spread, the total length of the basal arbor in each cell and the fraction of the arbor imaged in each cell, and further assuming that putative local dendritic spikes occur at random locations in the arbor, we estimate that ~2 putative local dendritic spikes occur across the basal arbor on each lap during the delay period in each cell. Taken together, these results suggest that the first step in the formation of many delayed onset place fields may be the occurrence of clustered synaptic input leading to sparse local dendritic spiking and local synaptic potentiation.

### Dendritic Inhibition Is Transiently Reduced during Exposure to Novel Environments

Due to the observations that most place fields appear during the first 8 laps in N, dendritic branch spiking in place fields is increased during this period and putative local dendritic spikes are occurring in dendrites prior to the formation of many delayed onset place fields, we asked whether changes in dendritic inhibition might influence these processes. Inhibition levels in the hippocampus are altered during exposure to novel environments (Wilson and McNaughton, 1993), although the specific interneuron subtypes involved remain unknown. We utilized somato-statin-Cre (SOM+) mice to obtain expression of GCaMP6f in a sub-population of interneurons (Lovett-Barron et al., 2014), which includes cells targeting the basal dendrites of CA1 pyramidal cells in the stratum oriens region (bistratified interneurons

[Goldberg and Coulter, 2013]), and imaged their axons in the stratum oriens, using the change in fluorescence across the axon population as a bulk measure of inhibition to the pyramidal cell dendritic region (Figure 4A).

Axonal  $\Delta F/F$  increased when mice transitioned from resting to running in F (Figure 4B;  $n = 3$  mice,  $n = 6$  sessions; mean resting  $\Delta F/F = 43.8\% \pm 0.1\%$ , mean running  $\Delta F/F = 118.3\% \pm 0.1\%$ ;  $p < 0.01$ , paired Student's t test), although their absolute velocity was not correlated to  $\Delta F/F$  (Figure 4C; slope not significant with 95% confidence bounds). We found that switching from F to N was associated with an abrupt decrease in mean axonal  $\Delta F/F$  during running (Figure 4F; mean  $\Delta F/F$  in the first eight laps in N =  $0.69 \pm 0.05$  SEM; each lap normalized to mean  $\Delta F/F$  in F in each case;  $p < 0.001$ , repeated-measures ANOVA with Tukey's post-test) that gradually returned to F levels (Figures 4D–4F;  $0.94 \pm 0.05$  SEM in the last eight laps in N;  $p > 0.05$  compared to F, repeated-measures ANOVA with Tukey's post-test). Importantly, these changes were not observed at the beginning of sessions when mice were first exposed to F (Figure S2G). These data demonstrate that the level of pyramidal neuron basal dendritic inhibition from SOM+ interneurons transiently decreases during initial exposure to a novel environment. Such a reduction could create a time window in which branch spikes and localized dendritic spikes induce synaptic potentiation, allowing specific sets of (potentiated) synapses to drive somatic firing in the place field once inhibition returns to F levels.

We next measured the level of somatic inhibition to CA1 pyramidal neurons during exposure to N. Parvalbumin-Cre mice were utilized to gain expression of GCaMP6f in basket cell axons using the same strategy as above for SOM+ axons. Axons from these interneurons form basket-like structures around CA1 pyramidal cell somata (Figure 4G). We measured mean changes in fluorescence of these axon structures as a bulk measure of somatic inhibition. As with SOM+ axons in the stratum oriens, basket cell axonal  $\Delta F/F$  increased when mice transitioned from resting to running in F (Figure 4H;  $n = 5$  mice,  $n = 9$  sessions; mean resting  $\Delta F/F = 38.9\% \pm 4.1\%$ , mean running  $\Delta F/F = 121.8\% \pm 10.2\%$ ;  $p < 0.001$ , paired t test), and their absolute velocity was also not correlated to  $\Delta F/F$  (Figure 4I; slope not significant with 95% confidence bounds). Basket cell axons surrounding pyramidal cell somata showed an abrupt increase in mean axonal  $\Delta F/F$  during running when the environment was switched from F to N (Figures 4J–4L; mean  $\Delta F/F$  in the first eight laps in N [each lap normalized to mean  $\Delta F/F$  in F in each case] =  $1.15 \pm 0.05$  SEM;  $p < 0.05$ , Repeated-measures ANOVA with Tukey's

(C) Mean velocity versus mean axonal  $\Delta F/F$  on each lap in F (six sessions). N.S., linear regression, slope not significantly different from 0.

(D) Bottom: single mouse behavior of track position versus time during F to N switch. Middle: axonal  $\Delta F/F$  during switch.

(E) Mean axonal  $\Delta F/F$  during running on each lap (normalized to the mean in F in each case) during F to N switch (6 switches;  $n = 3$  mice). Mean from all mice in red.

(F) Normalized Mean axonal  $\Delta F/F$  during running in F, laps 1–8 in N and laps 15–22 in N. Open circles represent each F to N switch. Repeated-measures ANOVA with Tukey's post-test, N.S.,  $p > 0.05$ .

(G) GCaMP6f-expressing PV+ interneuron cell bodies and axons in CA1 pyramidal cell layer *in vivo*.

(H) Mean PV+ interneuron axonal  $\Delta F/F$  (average over all axons in field) during running versus resting in F (paired t test). Open circle, means from 9 sessions in F from 5 mice (one mouse had only one F to N switch).

(I) Mean velocity versus mean axonal  $\Delta F/F$  on each lap in F (9 sessions). N.S., Linear regression, slope not significantly different from 0.

(J) Bottom: single mouse behavior of track position versus time during F to N switch. Middle: axonal  $\Delta F/F$  during switch.

(K) Mean axonal  $\Delta F/F$  during running on each lap (normalized to the mean in F in each case) during F to N switch (9 switches;  $n = 5$  mice). Mean from all mice in red.

(L) Normalized mean axonal  $\Delta F/F$  during running in F, laps 1–8 in N and laps 15–22 in N. Open circles represent each F to N switch. Repeated-measures ANOVA with Tukey's post-test, N.S.,  $p > 0.05$ .

post-test) that gradually returned to F levels (Figures 4J–4L;  $0.94 \pm 0.07$  SEM;  $p > 0.05$  compared to F, repeated-measures ANOVA with Tukey's post-test). Importantly, these changes were not observed at the beginning of sessions when mice were first exposed to F (Figure S2E). These data demonstrate that the level of pyramidal neuron somatic inhibition from PV+ interneurons transiently increases during initial exposure to a novel environment.

### NMDA Receptors in CA1 Pyramidal Neurons Are Required for the Formation of a Subset of Place Fields

To test the involvement of NMDA receptors in branch spiking, remapping, and place field formation during novel environment exposure, we used an inducible NMDA knockdown strategy. The gene encoding the NR1 subunit that is necessary for functional NMDA receptors can be knocked down in *Grin1<sup>lox/lox</sup>* mice (referred to here as NR1 mice) in a Cre-dependent manner (McHugh et al., 1996; Tsien et al., 1996). We therefore injected AAV-CaMKII-Cre along with AAV-Syn-flexed-GCaMP6f into the dorsal CA1 region of these mice to obtain Cre-dependent expression of GCaMP6f and Cre-dependent knockdown of NR1 exclusively in the same neurons (Figure S4A). We found that the fraction of place fields that formed in N was significantly reduced in populations of CA1 neurons with NR1 knocked down (Figures 5A–5C) compared to wild-type (WT) controls (fraction of place fields that formed from the active cell population in N:  $0.24 \pm 0.04$  SEM in WT controls versus  $0.11 \pm 0.05$  SEM in NR1 knockdown, chi-squared proportionality test,  $p < 0.05$ ), consistent with previous findings in which other components of the plasticity pathway were knocked out (Rotenberg et al., 1996). We found that transient durations were not different between the NR1 knockdown and WT populations and the maximum standard deviation of transients above the noise were slightly higher in the NR1 knockdown population (Figures S5A and S5B). Therefore, the reduction in place fields in the NR1 knockdown population could not be explained by a reduced ability to detect somatic transients compared to WT. We did observe a few differences in NR1 mouse behavior (decrease in running velocity and increase in stopping probability, Figures S4H–S4J) and a reduction in branch spiking in NR1 knockdown (sparse NR1 knockdown and GCaMP6f expression) compared to WT place cells (Figures S4E–S4G), but spatial correlations and place field onset lap (for the reduced number of place cells) appeared similar to WT (Figures S4B–S4D). Further, putative local dendritic spikes were not observed in NR1 knockdown place cells (sparse NR1 knockdown and GCaMP6f expression) during the delay period before somatic place fields formed; though ~8-fold fewer place cell dendrite recordings were available for analysis from the NR1 (fewer place cells with fewer dendrites) versus WT mice. Based on the frequency of putative local dendritic spikes observed in WT place cells, ~4 putative local dendritic spikes were expected from the NR1 knockdown recordings.

Interestingly, some of the place fields that formed in the NR1 knockdown population in N displayed a reduction in somatic firing frequency throughout the session (somatic calcium transients decreased in frequency throughout the session; Figure 5E), more so than in the WT population (Figure 5D). This sug-

gests that although place fields can form in CA1 pyramidal neurons in the absence of functional NMDA receptors, their ability to maintain place field firing over time is diminished. One possible explanation for this finding is that a lack of synaptic potentiation occurs in the dendrites of the NR1 knockdown population during the window of lowered inhibition upon initial exposure to N, which leads to an effective reduction in synaptic drive when inhibition returns to baseline levels. To further explore this hypothesis, we measured the number of detectable somatic transients during the first 8 laps in N and compared these numbers to the last 8 laps in N in all active neurons in both the NR1 knockdown and WT populations ( $n = 1,882$  neurons from  $n = 4$  WT mice;  $n = 835$  neurons from  $n = 3$  NR1 mice; estimated fraction of active cells in the field of view in WT =  $0.46 \pm 0.02$  SEM versus  $0.46 \pm 0.04$  SEM in NR1). We found that in both populations the number of transients was significantly higher during the first eight laps versus the last eight laps (Figure 5F; first eight laps WT =  $11.5 \pm 0.1$  SEM versus last eight laps WT =  $8.8 \pm 0.1$  SEM,  $p < 0.01$ , paired t test; first eight laps NR1 =  $11.1 \pm 0.2$  SEM versus last eight laps NR1 =  $6.6 \pm 0.2$  SEM,  $p < 0.05$ , paired t test; t tests with Bonferroni correction). Also, the number of transients during the first 8 laps was not different between the NR1 knock down and WT populations (Figure 5F; first eight laps WT =  $11.5 \pm 0.1$  SEM versus first eight laps NR1 =  $11.1 \pm 0.2$  SEM,  $p > 0.05$ , unpaired t test). However, there was a greater reduction in transient number in the last eight laps in the NR1 knockdown versus WT populations (Figure 5F, last eight laps WT =  $8.8 \pm 0.1$  SEM versus last eight laps NR1 =  $6.6 \pm 0.2$  SEM,  $p < 0.001$ , unpaired t test; t tests with Bonferroni correction). At the same time, no differences in transient amplitude or duration were observed between the NR1 knockdown and WT populations (Figures S5D and S5E). These results suggest that somatic firing is largely not dependent on functional NMDA receptors (Ekstrom et al., 2001; Kentros et al., 1998; McHugh et al., 1996) during the initial exposure to a novel environment. Instead, NMDA receptors may act to potentiate synapses during this period so that when dendritic inhibition returns to baseline levels these synapses become strong enough to drive somatic firing. This process may be necessary for the formation of a firing field in a subset of CA1 place fields, although in other cells across the CA1 population place fields can still form without NMDA-dependent synaptic potentiation (Figure S6).

### DISCUSSION

We propose the existence of two pathways that can lead to place field formation during exposure to novel environments. In the first, the sum of all synaptic inputs is large enough upon initial exposure to drive action potential firing at a particular location (the new place field; Figure S6, left). The other pathway is one in which the sum of all synaptic inputs is initially too small to drive somatic firing, but after a subset of inputs that are active at a particular location are potentiated, they become strong enough to drive somatic place field firing in the new place field (Figure S6, right). Supporting the idea that some place fields do not require synaptic plasticity to form, we found many place fields with somatic firing on the first lap in a novel environment. Although this somatic firing co-occurred with high levels of branch spiking,

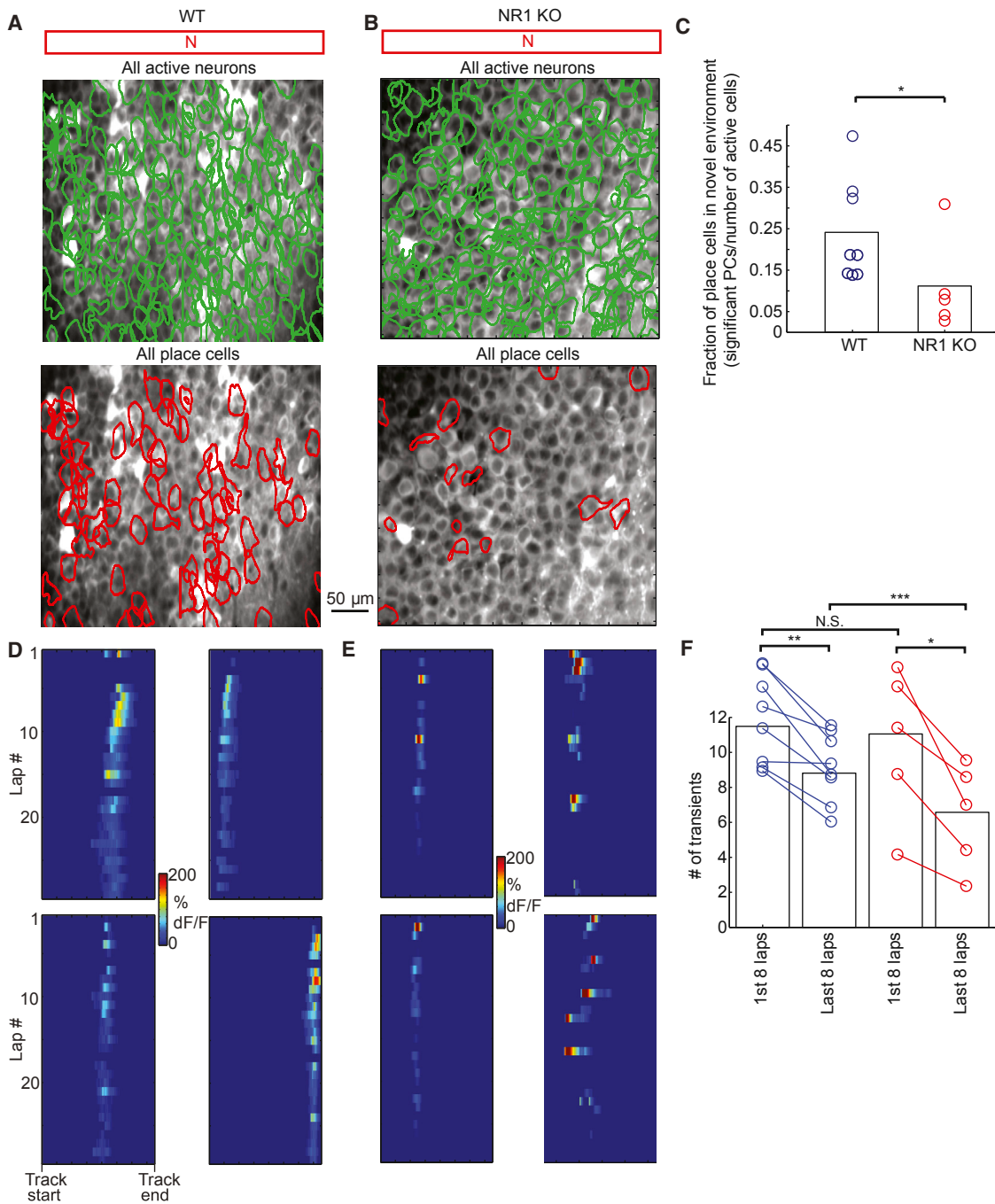


**Figure 5. NMDA Receptors in CA1 Pyramidal Neurons Are Required for the Formation of a Subset of Place Fields**

(A and B) GCaMP6f-expressing neurons in CA1 of WT (A) and NR1 (B, NMDA receptors functionally knocked out in GCaMP6f-expressing neurons) mouse. Top: all active neurons in the field of view in N (green). Bottom: all place cells encoding N (red).

(C) Fraction of the population of active cells in the field of view with a place field in N for WT versus NR1 mice. Open circles, fraction from individual fields of view. Bars, mean across all fields ( $n = 8$  fields from WT  $n = 5$  from NR1; from  $n = 4$  WT,  $n = 3$  NR1 mice). \*, chi-squared proportionality test,  $p < 0.05$ .

(D and E) Somatic place field transients shown lap by lap in N in WT mice (four in D) and NR1 mice with functional NMDA receptors knocked out of GCaMP6f-expressing cells (four in E); first row represents first traversal mouse ever made across N. Somatic place field calcium transients have higher dF/F amplitudes during initial laps and for cells lacking NMDA receptors, fields tend to disappear toward session end (E).

(F) Mean number of significant calcium transients detected from all active cells in WT mice ( $n = 4$  mice,  $n = 1,882$  transients; blue) and NR1 mice with functional NMDA receptors knocked out of GCaMP6f-expressing cells ( $n = 3$  mice;  $n = 835$  transients; red). Blue to red, unpaired t test, \*\*\* $p < 0.001$ ; N.S.,  $p > 0.05$ ; within color, paired t test, \*\* $p < 0.01$ , \* $p < 0.05$ ; all t tests with Bonferroni correction. Bars, mean from all transients across all mice. Open circles, means from each field of view.

any potentiation produced by these dendritic events could not have been required for the coincident firing in the new place field; instead, potentiation produced by these dendritic events may act to refine the fields further (see below). Supporting the case that synaptic plasticity is required to form many other place fields, we found localized putative dendritic spikes (likely NMDA spikes [Bandalis et al., 2016; Schiller et al., 2000]) occurring before detectable somatic firing on the first few laps of novel environment exposure. These putative local dendritic spikes likely potentiate small clusters of synapses, which over many minutes become strong enough to drive somatic firing and increased levels of branch spiking in a new place field. In further support of the idea that two different pathways can lead to new place fields, we found that knocking out NMDA receptors in a population of CA1 neurons reduced the number of place fields that formed across the population by ~50%. This suggests that approximately half of CA1 place fields require synaptic plasticity to form, and half do not.

In both of the proposed pathways for place field formation, nearly all place fields displayed high BSP when somatic firing first appeared. One possible purpose of this high BSP may be to refine place fields by strengthening co-occurring inputs throughout the arbor so that somatic firing becomes more spatially precise and place fields more temporally stable (Cacucci et al., 2007; Kentros et al., 1998; McHugh et al., 1996; Rotenberg et al., 1996; Sheffield and Dombeck, 2015). This is supported by NMDA-dependent plasticity perturbation experiments (Cacucci et al., 2007; Kentros et al., 1998; McHugh et al., 1996) in which the place fields that formed were less precise and less stable. Therefore, synaptic plasticity likely plays a fundamental role in the normal development of all place fields (Dragoi et al., 2003; Lever et al., 2002; Wilson and McNaughton, 1993), by stabilizing and refining them, but is additionally required for the formation of a subset of place fields (through local dendritic spike-induced potentiation). In both cases, these processes are likely influenced by the initial decrease in dendritic inhibition. The subsequent return of dendritic inhibition likely increases the amount of input required to drive any further synaptic changes, therefore closing the window for large amounts of synaptic plasticity to occur and stabilizing the synaptic changes that took place to encode the new environment.

Burst firing in CA1 pyramidal neurons, likely driven by coincident CA3 (onto CA1 basal, oblique, and proximal apical dendrites) and EC3 input (onto CA1 distal apical tuft dendrites), is associated with the formation of new place fields in familiar environments (Bittner et al., 2015). Synapses from multiple input pathways may become potentiated during burst events, leading to the binding of information across multiple input streams and allowing these synapses to drive firing on subsequent traversals in a new place field. Our data showing high levels of branch spike prevalence (BSP) when place fields first appear in novel environments support this idea. Indeed, high BSP in basal dendrites appears to be a dendritic measure indicating the occurrence of somatic burst firing in CA1 pyramidal neurons (Grienberger et al., 2014). It is therefore likely that somatic burst firing and high levels of BSP co-occur when somatic firing first appears in many place fields. However, we also found that the first appearance of a small percentage of place fields was associated with low levels

of BSP, suggesting that bursting, high levels of BSP and further binding of information across CA3 and EC3 are not necessary for the formation of all place fields. Furthermore, our observation of putative local dendritic spikes prior to the formation of detectable place field firing suggests that additional steps may be required to form place fields in many cells, with localized dendritic spikes starting the process by potentiating a small subset of synapses from one input stream or the other (CA3 or EC3). Once potentiated, these inputs can then drive place field firing, higher levels of BSP, and burst firing to recruit more inputs (possibly over behavior timescales [Bittner et al., 2017]) to make the fields more precise, stable, and possibly represent bound information across EC3 and CA3.

Local dendritic spikes have been shown to play functionally important roles *in vivo* (Cichon and Gan, 2015; Lavzin et al., 2012; Palmer et al., 2014; Sheffield and Dombeck, 2015; Smith et al., 2013), and in brain slices are capable of inducing synaptic potentiation (Bandalis et al., 2016; Golding et al., 2002; Gordon et al., 2006; Hardie and Spruston, 2009; Magee and Johnston, 1997; Weber et al., 2016). We estimate that ~2 putative local dendritic spikes occur across the basal dendritic arbor on each lap during the delay period prior to somatic place field appearance. It has been proposed that network information storage capacity is maximized when very few synapses are modified to store each new input pattern through localized dendritic spikes (Wu and Mel, 2009). This model also predicts that single branches that have undergone synaptic potentiation can then cause somatic firing. Our observations are consistent with these predictions, and part of the delay period that we observed in some place fields could be due to the time required for long-term potentiation to fully take effect (Hardie and Spruston, 2009; Murakoshi et al., 2011; Tigaret et al., 2016). This idea is partly supported by a recent somatic intracellular place cell recording study that found increasing subthreshold responses in novel virtual environments before somatic place field firing began (Cohen et al., 2017).

Our previous work fits with the idea that NMDA receptors are involved in refining place fields as we found that place fields with the highest BSP were more precise and stable in familiar environments (Sheffield and Dombeck, 2015), likely through their effect on alleviating Mg<sup>2+</sup> block of NMDA receptors in the presence of presynaptic input. This suggests that once a cognitive map has been established through the initial steps described above (Figure S6), the synapses that drive firing in individual place fields are maintained in strength by branch spikes each time the animal experiences the same environment (and also possibly offline through replay events). However, in addition to this role in refining fields, here we found that NMDA receptors are likely required for the formation of ~50% of place fields in novel environments. NMDA receptors in CA1 therefore likely serve many roles: forming place fields in novel environments through synaptic potentiation, refining place fields and making them more precise and stable, and maintaining the precision and stability of place fields over time in familiar environments by maintaining synaptic strength.

One possible explanation for how some place fields can form without synaptic potentiation is that some synapses are pre-strengthened prior to novel environment exposure and are activated during the experience to drive somatic place field firing.

Certain cells can be predicted to express place fields prior to exposure to a novel environment based on their participation in pre-play (Dragoi and Tonegawa, 2011, 2013a, 2013b), suggesting that experience-dependent synaptic plasticity plays little to no role in the appearance of these fields since their inputs are already able to drive firing prior to the experience. Place fields that engage pre-strengthened inputs could appear immediately upon exposure to novel environments, or even following a delayed period, as changes in attention could later activate these pathways (Monaco et al., 2014). It is also possible that NMDA-dependent synaptic plasticity occurs in presynaptic regions to drive some CA1 place field formation (Marr, 1971).

Similar to the findings here, differential inhibitory dynamics (differential changes in PV+ and SOM+ axonal boutons) have been observed in the motor cortex of mice during motor learning (Chen et al., 2015). Differential changes in inhibition across the somato-dendritic compartment during learning may be a general mechanism that supports the formation of new representations in the brain. Further, different interneuron subtypes may be involved in extracting different components of the learned representation (Lovett-Barron et al., 2014) and may be involved in routing information flow from CA3 and EC3 pathways during place field firing (Fernández-Ruiz et al., 2017).

Interestingly, significant differences were observed here between the F to N transitions compared to the F to F transitions (Figures 2, 4, and S2), suggesting that increased attention or environmental saliency may play a role in changing the functional state of circuits in CA1. Neuromodulatory pathways may control this process, with likely candidates including cholinergic (Has-selmo and McGaughy, 2004; Teles-Grilo Ruivo et al., 2017) and/or dopaminergic (Kentros et al., 2004) inputs.

## STAR★METHODS

Detailed methods are provided in the online version of this paper and include the following:

- KEY RESOURCES TABLE
- CONTACT FOR REAGENT AND RESOURCE SHARING
- EXPERIMENTAL MODEL AND SUBJECT DETAILS
  - Animals
- METHOD DETAILS
  - Mouse surgery and virus injections
  - Behavior and virtual reality switching
  - Two-photon imaging
  - Image processing
  - ROI selection and calcium transient analysis
  - Behavior analysis
  - Defining place fields
  - Place field spatial correlation
  - Place field onset lap
  - *In vivo* dendrite analysis
  - NMDA receptor knockdown
  - NMDA receptor knockdown immunohistochemistry
  - Hippocampal slice preparation
  - *In vitro* imaging and glutamate uncaging
- QUANTIFICATION AND STATISTICAL ANALYSIS
- DATA AND SOFTWARE AVAILABILITY

## SUPPLEMENTAL INFORMATION

Supplemental Information includes six figures and can be found with this article online at <https://doi.org/10.1016/j.neuron.2017.09.029>.

## AUTHOR CONTRIBUTIONS

M.E.J.S. performed *in vivo* experiments and analyzed data; M.D.A. performed *in vitro* experiments, a few *in vivo* experiments, and analyzed data. D.A.D. and M.E.J.S. discussed analysis strategies, designed experiments, and wrote the manuscript.

## ACKNOWLEDGMENTS

We thank members of the Dombeck lab for comments on the manuscript, S. Sato for immuno labeling suggestions, M. Bevan for NR1 mice, and V. Jayaraman, R. Kerr, D. Kim, L. Looger, and K. Svoboda from the GENIE Project (Janelia Farm, HHMI) for GCaMP6. This work was supported by The McKnight Foundation, The Klingenstein Foundation, The Whitehall Foundation, Northwestern University, The Chicago Biomedical Consortium with support from the Searle Funds at The Chicago Community Trust, The NIH (1R01MH101297, 1F31NS098666, and 2T32MH067564), NSF (CRCNS 1516235), and M.E.J.S. was an Ellison Medical Foundation Fellow of the Life Sciences Research Foundation.

Received: May 15, 2017

Revised: August 9, 2017

Accepted: September 19, 2017

Published: October 11, 2017

## REFERENCES

- Aronov, D., and Tank, D.W. (2014). Engagement of neural circuits underlying 2D spatial navigation in a rodent virtual reality system. *Neuron* 84, 442–456.
- Bittner, K.C., Grienberger, C., Vaidya, S.P., Milstein, A.D., Macklin, J.J., Suh, J., Tonegawa, S., and Magee, J.C. (2015). Conjunctive input processing drives feature selectivity in hippocampal CA1 neurons. *Nat. Neurosci.* 18, 1133–1142.
- Bittner, K.C., Milstein, A.D., Grienberger, C., Romani, S., and Magee, J.C. (2017). Behavioral time scale synaptic plasticity underlies CA1 place fields. *Science* 357, 1033–1036.
- Bliss, T.V., and Collingridge, G.L. (1993). A synaptic model of memory: long-term potentiation in the hippocampus. *Nature* 361, 31–39.
- Bloodgood, B.L., and Sabatini, B.L. (2007). Nonlinear regulation of unitary synaptic signals by CaV(2.3) voltage-sensitive calcium channels located in dendritic spines. *Neuron* 53, 249–260.
- Bloodgood, B.L., Giessel, A.J., and Sabatini, B.L. (2009). Biphasic synaptic Ca influx arising from compartmentalized electrical signals in dendritic spines. *PLoS Biol.* 7, e1000190.
- Bostock, E., Muller, R.U., and Kubie, J.L. (1991). Experience-dependent modifications of hippocampal place cell firing. *Hippocampus* 1, 193–205.
- Brandalise, F., Carta, S., Helmchen, F., Lisman, J., and Gerber, U. (2016). Dendritic NMDA spikes are necessary for timing-dependent associative LTP in CA3 pyramidal cells. *Nat. Commun.* 7, 13480.
- Cacucci, F., Wills, T.J., Lever, C., Giese, K.P., and O'Keefe, J. (2007). Experience-dependent increase in CA1 place cell spatial information, but not spatial reproducibility, is dependent on the autophosphorylation of the alpha-isozyme of the calcium/calmodulin-dependent protein kinase II. *J. Neurosci.* 27, 7854–7859.
- Carr, M.F., Jadhav, S.P., and Frank, L.M. (2011). Hippocampal replay in the awake state: a potential substrate for memory consolidation and retrieval. *Nat. Neurosci.* 14, 147–153.
- Chen, T.W., Wardill, T.J., Sun, Y., Pulver, S.R., Renninger, S.L., Baohan, A., Schreiter, E.R., Kerr, R.A., Orger, M.B., Jayaraman, V., et al. (2013). Ultrasensitive fluorescent proteins for imaging neuronal activity. *Nature* 499, 295–300.

- Chen, S.X., Kim, A.N., Peters, A.J., and Komiyama, T. (2015). Subtype-specific plasticity of inhibitory circuits in motor cortex during motor learning. *Nat. Neurosci.* 18, 1109–1115.
- Chu, H.Y., Atherton, J.F., Wokosin, D., Surmeier, D.J., and Bevan, M.D. (2015). Heterosynaptic regulation of external globus pallidus inputs to the subthalamic nucleus by the motor cortex. *Neuron* 85, 364–376.
- Cichon, J., and Gan, W.B. (2015). Branch-specific dendritic Ca(2+) spikes cause persistent synaptic plasticity. *Nature* 520, 180–185.
- Cohen, J.D., Bolstad, M., and Lee, A.K. (2017). Experience-dependent shaping of hippocampal CA1 intracellular activity in novel and familiar environments. *eLife* 6, 6.
- Deguchi, Y., Donato, F., Galimberti, I., Cabuy, E., and Caroni, P. (2011). Temporally matched subpopulations of selectively interconnected principal neurons in the hippocampus. *Nat. Neurosci.* 14, 495–504.
- Dombeck, D.A., Khabbaz, A.N., Collman, F., Adelman, T.L., and Tank, D.W. (2007). Imaging large-scale neural activity with cellular resolution in awake, mobile mice. *Neuron* 56, 43–57.
- Dombeck, D.A., Harvey, C.D., Tian, L., Looger, L.L., and Tank, D.W. (2010). Functional imaging of hippocampal place cells at cellular resolution during virtual navigation. *Nat. Neurosci.* 13, 1433–1440.
- Dragoi, G., and Tonegawa, S. (2011). Preplay of future place cell sequences by hippocampal cellular assemblies. *Nature* 469, 397–401.
- Dragoi, G., and Tonegawa, S. (2013a). Distinct preplay of multiple novel spatial experiences in the rat. *Proc. Natl. Acad. Sci. USA* 110, 9100–9105.
- Dragoi, G., and Tonegawa, S. (2013b). Selection of preconfigured cell assemblies for representation of novel spatial experiences. *Philos. Trans. R. Soc. Lond. B Biol. Sci.* 369, 20120522.
- Dragoi, G., Harris, K.D., and Buzsáki, G. (2003). Place representation within hippocampal networks is modified by long-term potentiation. *Neuron* 39, 843–853.
- Ekstrom, A.D., Meltzer, J., McNaughton, B.L., and Barnes, C.A. (2001). NMDA receptor antagonism blocks experience-dependent expansion of hippocampal “place fields”. *Neuron* 31, 631–638.
- Fernández-Ruiz, A., Oliva, A., Nagy, G.A., Maurer, A.P., Berényi, A., and Buzsáki, G. (2017). Entorhinal-CA3 dual-input control of spike timing in the hippocampus by theta-gamma coupling. *Neuron* 93, 1213–1226.e5.
- Foster, D.J., and Wilson, M.A. (2006). Reverse replay of behavioural sequences in hippocampal place cells during the awake state. *Nature* 440, 680–683.
- Frank, L.M., Stanley, G.B., and Brown, E.N. (2004). Hippocampal plasticity across multiple days of exposure to novel environments. *J. Neurosci.* 24, 7681–7689.
- Fyhn, M., Hafting, T., Treves, A., Moser, M.B., and Moser, E.I. (2007). Hippocampal remapping and grid realignment in entorhinal cortex. *Nature* 446, 190–194.
- Goldberg, E.M., and Coulter, D.A. (2013). Mechanisms of epileptogenesis: a convergence on neural circuit dysfunction. *Nat. Rev. Neurosci.* 14, 337–349.
- Golding, N.L., Staff, N.P., and Spruston, N. (2002). Dendritic spikes as a mechanism for cooperative long-term potentiation. *Nature* 418, 326–331.
- Gordon, U., Polksky, A., and Schiller, J. (2006). Plasticity compartments in basal dendrites of neocortical pyramidal neurons. *J. Neurosci.* 26, 12717–12726.
- Grienberger, C., Chen, X., and Konnerth, A. (2014). NMDA receptor-dependent multidendrite Ca(2+) spikes required for hippocampal burst firing in vivo. *Neuron* 81, 1274–1281.
- Hardie, J., and Spruston, N. (2009). Synaptic depolarization is more effective than back-propagating action potentials during induction of associative long-term potentiation in hippocampal pyramidal neurons. *J. Neurosci.* 29, 3233–3241.
- Hasselmo, M.E., and McGaughy, J. (2004). High acetylcholine levels set circuit dynamics for attention and encoding and low acetylcholine levels set dynamics for consolidation. *Prog. Brain Res.* 145, 207–231.
- Heys, J.G., Rangarajan, K.V., and Dombeck, D.A. (2014). The functional micro-organization of grid cells revealed by cellular-resolution imaging. *Neuron* 84, 1079–1090.
- Hill, A.J. (1978). First occurrence of hippocampal spatial firing in a new environment. *Exp. Neurol.* 62, 282–297.
- Kentros, C., Hargreaves, E., Hawkins, R.D., Kandel, E.R., Shapiro, M., and Muller, R.V. (1998). Abolition of long-term stability of new hippocampal place cell maps by NMDA receptor blockade. *Science* 280, 2121–2126.
- Kentros, C.G., Agnihotri, N.T., Streater, S., Hawkins, R.D., and Kandel, E.R. (2004). Increased attention to spatial context increases both place field stability and spatial memory. *Neuron* 42, 283–295.
- Lavzin, M., Rapoport, S., Polksky, A., Garion, L., and Schiller, J. (2012). Nonlinear dendritic processing determines angular tuning of barrel cortex neurons in vivo. *Nature* 490, 397–401.
- Lee, D., Lin, B.J., and Lee, A.K. (2012). Hippocampal place fields emerge upon single-cell manipulation of excitability during behavior. *Science* 337, 849–853.
- Leutgeb, S., Leutgeb, J.K., Treves, A., Moser, M.B., and Moser, E.I. (2004). Distinct ensemble codes in hippocampal areas CA3 and CA1. *Science* 305, 1295–1298.
- Leutgeb, S., Leutgeb, J.K., Barnes, C.A., Moser, E.I., McNaughton, B.L., and Moser, M.B. (2005). Independent codes for spatial and episodic memory in hippocampal neuronal ensembles. *Science* 309, 619–623.
- Lever, C., Wills, T., Cacucci, F., Burgess, N., and O’Keefe, J. (2002). Long-term plasticity in hippocampal place-cell representation of environmental geometry. *Nature* 416, 90–94.
- Losonczy, A., and Magee, J.C. (2006). Integrative properties of radial oblique dendrites in hippocampal CA1 pyramidal neurons. *Neuron* 50, 291–307.
- Losonczy, A., Makara, J.K., and Magee, J.C. (2008). Compartmentalized dendritic plasticity and input feature storage in neurons. *Nature* 452, 436–441.
- Lovett-Barron, M., Kaifosh, P., Kheirbek, M.A., Danielson, N., Zaremba, J.D., Reardon, T.R., Turi, G.F., Hen, R., Zemelman, B.V., and Losonczy, A. (2014). Dendritic inhibition in the hippocampus supports fear learning. *Science* 343, 857–863.
- Magee, J.C., and Johnston, D. (1997). A synaptically controlled, associative signal for Hebbian plasticity in hippocampal neurons. *Science* 275, 209–213.
- Major, G., Polksky, A., Denk, W., Schiller, J., and Tank, D.W. (2008). Spatiotemporally graded NMDA spike/plateau potentials in basal dendrites of neocortical pyramidal neurons. *J. Neurophysiol.* 99, 2584–2601.
- Marr, D. (1971). Simple memory: a theory for archicortex. *Philos. Trans. R. Soc. Lond. B Biol. Sci.* 262, 23–81.
- McHugh, T.J., Blum, K.I., Tsien, J.Z., Tonegawa, S., and Wilson, M.A. (1996). Impaired hippocampal representation of space in CA1-specific NMDAR1 knockout mice. *Cell* 87, 1339–1349.
- Milojkovic, B.A., Zhou, W.L., and Antic, S.D. (2007). Voltage and calcium transients in basal dendrites of the rat prefrontal cortex. *J. Physiol.* 585, 447–468.
- Miri, A., Daie, K., Burdine, R.D., Aksay, E., and Tank, D.W. (2011). Regression-based identification of behavior-encoding neurons during large-scale optical imaging of neural activity at cellular resolution. *J. Neurophysiol.* 105, 964–980.
- Monaco, J.D., Rao, G., Roth, E.D., and Knierim, J.J. (2014). Attentive scanning behavior drives one-trial potentiation of hippocampal place fields. *Nat. Neurosci.* 17, 725–731.
- Morris, R.G., Garrud, P., Rawlins, J.N., and O’Keefe, J. (1982). Place navigation impaired in rats with hippocampal lesions. *Nature* 297, 681–683.
- Morris, R.G., Anderson, E., Lynch, G.S., and Baudry, M. (1986). Selective impairment of learning and blockade of long-term potentiation by an N-methyl-D-aspartate receptor antagonist, AP5. *Nature* 319, 774–776.
- Mukamel, E.A., Nimmerjahn, A., and Schnitzer, M.J. (2009). Automated analysis of cellular signals from large-scale calcium imaging data. *Neuron* 63, 747–760.
- Muller, R.U., and Kubie, J.L. (1987). The effects of changes in the environment on the spatial firing of hippocampal complex-spike cells. *J. Neurosci.* 7, 1951–1968.

- Murakoshi, H., Wang, H., and Yasuda, R. (2011). Local, persistent activation of Rho GTPases during plasticity of single dendritic spines. *Nature* 472, 100–104.
- O’Keefe, J., and Dostrovsky, J. (1971). The hippocampus as a spatial map. Preliminary evidence from unit activity in the freely-moving rat. *Brain Res.* 34, 171–175.
- Oakley, J.C., Schwindt, P.C., and Crill, W.E. (2001). Initiation and propagation of regenerative Ca(2+)-dependent potentials in dendrites of layer 5 pyramidal neurons. *J. Neurophysiol.* 86, 503–513.
- Palmer, L.M., Shai, A.S., Reeve, J.E., Anderson, H.L., Paulsen, O., and Larkum, M.E. (2014). NMDA spikes enhance action potential generation during sensory input. *Nat. Neurosci.* 17, 383–390.
- Pologruto, T.A., Sabatini, B.L., and Svoboda, K. (2003). ScanImage: flexible software for operating laser scanning microscopes. *Biomed. Eng. Online* 2, 13.
- Rotenberg, A., Mayford, M., Hawkins, R.D., Kandel, E.R., and Muller, R.U. (1996). Mice expressing activated CaMKII lack low frequency LTP and do not form stable place cells in the CA1 region of the hippocampus. *Cell* 87, 1351–1361.
- Sadowski, J.H., Jones, M.W., and Mellor, J.R. (2016). Sharp-wave ripples orchestrate the induction of synaptic plasticity during reactivation of place cell firing patterns in the hippocampus. *Cell Rep.* 14, 1916–1929.
- Schiller, J., Schiller, Y., and Clapham, D.E. (1998). NMDA receptors amplify calcium influx into dendritic spines during associative pre- and postsynaptic activation. *Nat. Neurosci.* 1, 114–118.
- Schiller, J., Major, G., Koester, H.J., and Schiller, Y. (2000). NMDA spikes in basal dendrites of cortical pyramidal neurons. *Nature* 404, 285–289.
- Seong, H.J., Behnia, R., and Carter, A.G. (2014). Impact of subthreshold membrane potential on synaptic responses at dendritic spines of layer 5 pyramidal neurons in the prefrontal cortex. *J. Neurophysiol.* 111, 1960–1972.
- Sheffield, M.E., and Dombeck, D.A. (2015). Calcium transient prevalence across the dendritic arbor predicts place field properties. *Nature* 517, 200–204.
- Silva, A.J., Paylor, R., Wehner, J.M., and Tonegawa, S. (1992). Impaired spatial learning in alpha-calcium-calmodulin kinase II mutant mice. *Science* 257, 206–211.
- Smith, S.L., Smith, I.T., Branco, T., and Häusser, M. (2013). Dendritic spikes enhance stimulus selectivity in cortical neurons *in vivo*. *Nature* 503, 115–120.
- Takeuchi, T., Duszkievicz, A.J., and Morris, R.G. (2013). The synaptic plasticity and memory hypothesis: encoding, storage and persistence. *Philos. Trans. R. Soc. Lond. B Biol. Sci.* 369, 20130288.
- Teles-Grilo Ruivo, L.M., Baker, K.L., Conway, M.W., Kinsley, P.J., Gilmour, G., Phillips, K.G., Isaac, J.T., Lowry, J.P., and Mellor, J.R. (2017). Coordinated acetylcholine release in prefrontal cortex and hippocampus is associated with arousal and reward on distinct timescales. *Cell Rep.* 18, 905–917.
- Teng, E., and Squire, L.R. (1999). Memory for places learned long ago is intact after hippocampal damage. *Nature* 400, 675–677.
- Tigaret, C.M., Olivo, V., Sadowski, J.H., Ashby, M.C., and Mellor, J.R. (2016). Coordinated activation of distinct Ca(2+) sources and metabotropic glutamate receptors encodes Hebbian synaptic plasticity. *Nat. Commun.* 7, 10289.
- Tsien, J.Z., Huerta, P.T., and Tonegawa, S. (1996). The essential role of hippocampal CA1 NMDA receptor-dependent synaptic plasticity in spatial memory. *Cell* 87, 1327–1338.
- van de Ven, G.M., Trouche, S., McNamara, C.G., Allen, K., and Dupret, D. (2016). Hippocampal Offline Reactivation Consolidates Recently Formed Cell Assembly Patterns during Sharp Wave-Ripples. *Neuron* 92, 968–974.
- Weber, J.P., Andrásfalvy, B.K., Polito, M., Magó, Á., Ujfalussy, B.B., and Makara, J.K. (2016). Location-dependent synaptic plasticity rules by dendritic spine cooperativity. *Nat. Commun.* 7, 11380.
- Wei, D.S., Mei, Y.A., Bagal, A., Kao, J.P., Thompson, S.M., and Tang, C.M. (2001). Compartmentalized and binary behavior of terminal dendrites in hippocampal pyramidal neurons. *Science* 293, 2272–2275.
- Wilson, M.A., and McNaughton, B.L. (1993). Dynamics of the hippocampal ensemble code for space. *Science* 261, 1055–1058.
- Wilson, M.A., and McNaughton, B.L. (1994). Reactivation of hippocampal ensemble memories during sleep. *Science* 265, 676–679.
- Wu, X.E., and Mel, B.W. (2009). Capacity-enhancing synaptic learning rules in a medial temporal lobe online learning model. *Neuron* 62, 31–41.

**STAR★METHODS****KEY RESOURCES TABLE**

REAGENT or RESOURCE	SOURCE	IDENTIFIER
<b>Antibodies</b>		
Rabbit polyclonal anti-GluN1 IgG	abcam	RRID: AB_776808
Goat anti-Rabbit IgG (H+L) Highly Cross-Adsorbed Secondary Antibody, Alexa Fluor 594	ThermoFisher Scientific	Cat#: A-110937
<b>Bacterial and Virus Strains</b>		
AAV1.CamKII0.4.Cre.SV40	Penn Vector Core	Cat#: AV-1-PV2396
AAV1.Syn.Flex.GCaMP6f.WPRE.SV40	Penn Vector Core	Cat#: AV-1-PV2819
AAV1.Syn.Flex.GCaMP6s.WPRE.SV40	Penn Vector Core	Cat#: AV-1-PV2821
AAV1.Syn.GCaMP6f.WPRE.SV40	Penn Vector Core	Cat#: AV-1-PV2822
<b>Chemicals, Peptides, and Recombinant Proteins</b>		
MNI-caged L glutamate (4-methoxy-7-nitroindolinyl-caged L-glutamate)	Tocris	Cat#: 1490
Tetrodotoxin (TTX)	Tocris	Cat#: 1078
SR-95531 hydrobromide (GABA <sub>A</sub> receptor antagonist)	Tocris	Cat# 1262
<b>Experimental Models: Organisms/Strains</b>		
Mouse: WT: C57BL/6J	The Jackson Laboratory	RRID: IMSR_JAX:000664
Mouse: PV-Cre: B6;129P2-Pvalb <sup>tm1(cre)Arbr</sup> /J	The Jackson Laboratory	RRID: IMSR_JAX:008069
Mouse: SOM-Cre: Sst <sup>tm2.1(cre)Zjh</sup> /J	The Jackson Laboratory	RRID: IMSR_JAX:013044
Mouse: NR1: B6.129S4-Grin1 <sup>tm2Stl</sup> /J	The Jackson Laboratory	RRID: IMSR_JAX:005246
<b>Software and Algorithms</b>		
MATLAB (Versions R2012a and R2013b)	MathWorks	RRID: SCR_001622
ScanImage 4	Pologruto et al., 2003	RRID: SCR_014307

**CONTACT FOR REAGENT AND RESOURCE SHARING**

Further information and requests for resources and reagents should be directed to and will be fulfilled by the Lead Contact, Daniel Dombeck, [d-dombeck@northwestern.edu](mailto:d-dombeck@northwestern.edu).

**EXPERIMENTAL MODEL AND SUBJECT DETAILS****Animals**

10 to 12 weeks old male C57BL/6 (WT), B6;129P2-Pvalb<sup>tm1(cre)Arbr</sup>/J (PV-Cre), Sst<sup>tm2.1(cre)Zjh</sup>/J (SOM-cre) and B6.129S4-Grin1<sup>tm2Stl</sup>/J (NR1) mice (20-30 g) were individually housed under a reverse 12 hr light / dark cycle. All experiments were approved by the Northwestern University Animal Care and Use Committee. Behavioral experiments were conducted during the animal's dark cycle.

**METHOD DETAILS****Mouse surgery and virus injections**

Mice were anesthetized (~1%–2% Isoflurane) and a small (~0.5–1.0 mm) craniotomy was made over the hippocampus (1.8 mm lateral, 2.3 mm caudal of Bregma). For single cell dendritic imaging a low titer Cre -virus (AAV1-CamKII-Cre, 1.5x10<sup>8</sup> GC/mL, all virus from University of Pennsylvania Vector Core) was injected (1 injection of ~30 nL at a depth of ~1250 µm below the dural surface using a beveled glass micropipette: ~1-2 MΩ after beveling) in combination with a high titer of flexed-GCaMP6 virus ((Chen et al., 2013) AAV1-Syn-flex-GCaMP6f or s, 1.4x10<sup>13</sup> GC/mL) leading to expression of GCaMP-6 in a sparse CA1 pyramidal neuron population. For population imaging, dense labeling was performed the same as sparse except only AAV1-Syn-GCaMP6f (1.5x10<sup>13</sup> GC/mL) was injected. For interneuron SOM+ or PV+ axon imaging, we injected a high titer of flexed-GCaMP6f virus (AAV1-Syn-flex-GCaMP6f, 1.4x10<sup>13</sup> GC/mL, ~30 nL) into the hippocampus of SOM+ or PV+ cre mice. Mouse water scheduling began the day after

virus injections (0.8–1.0 mL/day, and continued through all training and experiments) followed ~7 days later by a hippocampal window and head-plate implantation surgery (as described in ([Dombeck et al., 2010](#))). For live slice imaging and glutamate uncaging experiments, mice were injected following the same sparse labeling protocol and allowed to recover for 3 to 4 weeks prior to hippocampal slice preparation.

### Behavior and virtual reality switching

We used the same virtual reality and treadmill set-up as previously described ([Heys et al., 2014](#)), consisting of a 1D treadmill and a view angle within the virtual environment straight down the track. Training in a 3 m virtual linear track (F1; [Figure S1](#); one ~40–60 minute session per mouse per day) began ~7 days after window implantation and continued until mice routinely ran along F1 to achieve a high reward rate (>~2 rewards/minute); rewards in F1 consisted of water (4 µl) delivered as described previously ([Dombeck et al., 2010](#)). Mice were teleported back to the beginning of the track after each reward and after a short (1.5 s) delay. Once this criterion was reached (~5–7 days of virtual reality training in F1), imaging commenced the following day (experimental day 1). [Figure S1A](#) shows the experimental timeline that each mouse underwent. Experimental day 1 consisted of mice running at least 15 laps in F1, at which point the virtual environment was switched to a novel environment (N1). This VR switch occurred rapidly (~33ms) and was triggered while mice were at the start of the F1 track. Rewards in N1 were delivered at the end of the track as in F1, but consisted of 8 µl instead of 4 µl water rewards. Mice were then allowed to traverse the track for at least 20 laps before being placed back into their home cage. 24 hours later, on experimental day 2, mice were placed back into the same environment, N1, and allowed to traverse the track for at least 20 laps. This environment was now considered familiar, F2, at which point the environment was switched to a second novel environment, N2. Water rewards in N2 were 8 µl, and mice completed at least 20 laps before being placed in their home cage. 24 hours later, on experimental day 3, mice were placed back in N2 and completed at least 15 laps, at which point N2 was considered familiar, F3. Data from the two familiar environments prior to VR switch, F1 and F2, were grouped together and referred to as F throughout the main text and figures. Data from the two novel environments following VR switch, N1 and N2, were grouped together and referred to as either N throughout the main text and figures. No differences in the results reported here were observed between the first switch (F1 to N1) and the second switch (F2 to N2), justifying their grouping.

### Two-photon imaging

A Moveable Objective Microscope (Sutter Instruments) was customized for our imaging experiments. The microscope consisted of a resonant scanning module (Thorlabs), a 40 × /0.80 NA water immersion objective (LUCPlanFL N, Olympus) and enhanced collection optics. Green GCaMP6 fluorescence was routed to a GaAsP PMT (H10770PA-40) using a series of dichroic mirrors and band-pass filters (in order after leaving the back aperture; Semrock): FF665-Di02 long pass dichroic, FF01-680/sp short pass filter, FF560-Di01 long pass dichroic, FF01-510/84 band-pass filter. Stray light from the virtual reality monitor was blocked using a custom box surrounding the top of the microscope objective and the overlying dichroic mirror (not including the tube lens, scan lens, galvos or routing mirrors). This box had one hole on top, for entry of the excitation beam, which was covered with a color glass filter (FGL780, Thorlabs) and one hole on bottom for the microscope objective. This bottom hole was sealed using the same loose black rubber tube and tight fitting metal rings described previously ([Dombeck et al., 2010](#)). ScanImage 4 was used for microscope control and acquisition ([Pologruto et al., 2003](#)). Ti:Sapphire laser (Chameleon Ultra II, Coherent) light at 890 (for GCaMP6s) or 920 (for GCaMP6f) nm was used as the excitation source. Laser average power at the sample (after the objective) was 70–100 mW. A pockels cell (350-80-LA-BK-02, 302RM driver, Conoptics) was used to blank laser excitation at the edges of the field of view. Time-series movies (1024 or 512x256 pixels) were acquired at 50 Hz for single plane (population and interneuron axon imaging), 25 Hz for 2 plane and 12.5 Hz for 4 plane (dendrite imaging using an electric lens, see ([Sheffield and Dombeck, 2015](#))) acquisitions. A Digidata1440A (Molecular Devices) data acquisition system was used to record (Clampex 10.3) and synchronize position in the linear track, reward timing, and two-photon image frame timing.

### Image processing

Time-series movies for multi-plane recording were acquired using interleaved frames (i.e., every other frame was from the same plane for 2-plane imaging). The electric lens settling time of ~5 ms sometimes created distortions in the first few lines of each frame of the movie; these lines were therefore removed before subsequent analysis. Each multi-plane time-series was then split into separate time-series movies, one for each acquired plane. Each single-plane time-series, including those from population imaging, was then independently motion corrected using whole frame cross-correlation, as described previously ([Dombeck et al., 2010; Miri et al., 2011; Sheffield and Dombeck, 2015](#)). To decrease the motion correction time and increase the stability of the motion corrected movie, all time series movies from multiplane and single plane acquisitions were cropped in the x and y dimensions around an area containing structures with high baseline fluorescence that changed little throughout the movie. The x and y shifts for each frame calculated from the cropped movie was then applied to the original non-cropped movie. These motion corrected movies were then used for subsequent analysis. After time-series imaging, z series were acquired from each field of view from the external capsule fiber surface through the proximal apical dendrite.

### ROI selection and calcium transient analysis

For single cell imaging (sparse labeling) ROIs were selected by hand on the mean soma or dendrite images (mean time projection of all frames in the motion corrected time-series at each plane). ROIs were drawn to closely follow the outline of the structure of interest (soma or dendrite). Dendrites belonging to the co-imaged parent soma were identified offline by tracing them to the soma in the z series; additional verification was provided by their often co-occurring significant calcium transients with the soma.

For interneuron axon imaging in the Stratum Oriens (SOM+ mice) and pyramidal cell layer (PV+ mice), ROIs were selected by hand around an area containing a high density of axons in the image, avoiding somata and dendrites and minimizing areas with an absence of structure.

For population imaging, ROIs were defined as previously described (Mukamel et al., 2009) ( $\mu = 0.6$ , 150 principal components, 150 independent components, s.d. threshold = 2.5, s.d. smoothing width = 1, area limits = 100-1200 pixels). As seen previously (Dombeck et al., 2010), ROIs nearly always defined single cell regions. To calculate the average population  $\Delta F/F$  (Figures S2A and S2B), we selected a single ROI encompassing the entire FOV.

From dendrite and population time-series,  $\Delta F/F$  versus time traces were generated for each ROI as previously described (Dombeck et al., 2010). Briefly, slow changes in the fluorescence traces were removed by examining the distribution of fluorescence in a ~6 s interval around each sample in the trace and normalized by the 8th percentile value. These baseline corrected soma and dendrite fluorescence traces were then subjected to the analysis of the ratio of positive to negative going transients of various amplitudes and durations described previously (Dombeck et al., 2007). We used this analysis to identify significant transients with < 0.01% (< 0.001% for dendrites) false positive error rates; these identified significant transients were used in the subsequent analysis.

The somatic  $\Delta F/F$  traces consisted of a baseline interrupted periodically by calcium transients of varying amplitude, consistent with a difference in the number of underlying APs, and varied in duration, consistent with the summation of multiple transients (Dombeck et al., 2010; Sheffield and Dombeck, 2015). Dendritic calcium transients were consistent with those observed previously (Sheffield and Dombeck, 2015).

To avoid subtracting any slow changes in the fluorescence traces from interneuron axons, which have a baseline firing rate that could slowly vary with behavior and cause slow changes in fluorescence, time-series  $\Delta F/F$  traces were generated for each ROI by examining the distribution of fluorescence from the entire trace and normalizing each sample in the trace by the 8<sup>th</sup> percentile value (i.e., no removal of slow baseline variations). Measurements of  $\Delta F/F$  in Figure 4 are calculated from these baseline corrected traces.

### Behavior analysis

To calculate mean lap virtual velocity (Figure 1B; Figures 4C and 4I) for each lap, we divided the track length (3 m) by the time taken to traverse the track. Stopping periods or slow moving periods were included in this measure. To calculate stopping probability on each lap, we used an instantaneous virtual velocity threshold of 1 cm<sup>-s</sup>. If instantaneous virtual velocity fell below this threshold for at least 100 ms, we considered this a stopping period, and the probability of stopping on that lap was given a value of 1, regardless of whether additional stopping periods occurred on that lap. The lap stopping time was calculated from these stopping periods, and if mice stopped multiple times on a single lap, the total time stopped was summed together from each stopping period on that lap. We used the same virtual velocity threshold to classify running versus resting behavior (Figures 4B and 4H).

### Defining place fields

Place fields were identified and defined as described previously (Dombeck et al., 2010) with minor changes outlined below. Place fields were defined solely based on somatic calcium transients. First, long running periods were defined in which mouse movement along the virtual track consisted of virtual velocity > ~7 cm<sup>-s</sup> and run length > 40 cm without hitting the end of the track. The mean somatic  $\Delta F/F$  was calculated as a function of virtual track position for 150 position bins and this mean fluorescence versus position plot was then averaged over 3 adjacent points. Potential place fields were first identified as contiguous regions of this plot in which all of the points were greater than 25% of the difference between the peak somatic  $\Delta F/F$  value (for all 150 bins) and the baseline value (mean of the lowest 20 out of 150 somatic  $\Delta F/F$  values). These potential place field regions then had to satisfy the following criteria: 1. The field must be > 20 cm in width, 2. The field must have one value of at least 10% mean  $\Delta F/F$ , 3. The mean in field  $\Delta F/F$  value must be > 4 times the mean out of field  $\Delta F/F$  value and 4. Significant calcium transients must be present > 40% of the time the mouse spent in the place field. Potential place field regions that met these criteria were then defined as place fields if their p value from boot strapping was < 0.05, as described previously (Dombeck et al., 2010). These place fields were then treated independently, and transients that occurred outside of the defined place field region were removed for analysis of each specific field. The resultant place field was then used in all subsequent analysis. Place cells with multiple potential place field regions were treated in the same way, with each potential place field region treated independently and subjected to the same tests as above, except the mean out of field  $\Delta F/F$  value excluded  $\Delta F/F$  values from other potential place field regions. We only included place fields in which neither edge of the identified field was at the track start or track end.

### Place field spatial correlation

To measure place field spatial correlation across environments, we found place cells that had place fields in both environments and compared their mean place fields. Each place field pair to be compared was split into 150 position bins (2cm/bin) from which we calculated a Pearson's correlation coefficient, our measure of spatial correlation between 2 place fields. To measure place field

spatial correlation within environments, we first divided the session up into two halves based on the total number of laps completed within the session. We calculated a mean place field from transients that occurred within the first half of all the laps in that session, and a second mean place field from transients that occurred within the second half of that session. These two place fields then underwent the same spatial correlation test as above.

### Place field onset lap

To determine place field onset lap (Figures 1E and 1F, 2F), starting on lap 1 we searched for a significant somatic  $\Delta F/F$  calcium transient present within the boundaries of the previously determined mean place field calculated from all the laps in the session. If one were found we would then search for somatic  $\Delta F/F$  calcium transients on each of the next 5 laps. If 4 of the 6 laps had somatic  $\Delta F/F$  calcium transients within the mean place field boundaries, lap 1 would be considered the place field onset lap. If either lap 1 had no somatic  $\Delta F/F$  calcium transient or less than 4 of the 6 laps had somatic  $\Delta F/F$  calcium transients, we would move to lap 2 and repeat the search.

To determine place field onset lap in F (Figure 1F2), we trained a separate set mice as described above. In these mice, on experimental day 1, we began imaging the CA1 population prior to the first traversal of F on that day (this imaging procedure was repeated for the data acquired in Figures S2C–S2J).

### In vivo dendrite analysis

Identification of branch spikes, definition of branch spike prevalence (Figure 2) and analysis of dendritic area of significant  $\Delta F/F$  increase (Figure 3 and Figure S3) was the same as previously described (Sheffield and Dombeck, 2015). Additionally, significant dendrite localized calcium transients had to consist of at least 2 contiguous samples in the trace to be included. To prevent calcium transients from dendrites belonging to other cells in the FOV from potentially contaminating our dendrite  $\Delta F/F$  traces, we excluded from analysis periods when other cells in the FOV had significant somatic calcium transients. This step likely leads to missing some dendrite localized calcium transients, but eliminates false positives caused by calcium transients from other neurons.

Track location of dendrite localized transients (Figure 3D) was determined by finding the track location where the peak of the dendritic transient occurred. We then calculated the track distance between this location and the location of the mean somatic place field's weighted center of mass (see (Sheffield and Dombeck, 2015)). This distance was then normalized by the mean somatic place field width in each case.

We imaged both GCaMP6f-expressing ( $n = 12$  place fields) and GCaMP6s-expressing dendrites ( $n = 6$  place fields). Imaging at 920 nm, we found the baseline fluorescence signal in the GCaMP6s-expressing dendrites was oftentimes undetectable. Since unbound GCaMP6s emission is larger when excited by shorter wavelengths, we used 890 nm for all imaging experiments using GCaMP6s. This increased the signal from dendrites at rest, but resulted in reduced  $\Delta F/F$  transient amplitudes. Dendrite localized calcium transient max amplitudes during the delay period were therefore smaller in GCaMP6s-expressing dendrites compared to GCaMP6f-expressing dendrites (GCaMP6s amplitudes:  $114.6 \pm 25.6\% \Delta F/F$  versus GC6f amplitudes:  $224.2 \pm 25.1\% \Delta F/F$ , t test,  $p = 0.0002$ ). However, the number of dendrite localized calcium transients detected during the delay period was similar (GCaMP6s:  $n = 14$ ; GCaMP6f:  $n = 16$ ), and the transient durations (defined by the full width half max of the significant transients) were also not significantly different (GCaMP6s duration:  $230.8 \pm 8.1$  SEM ms versus GCaMP6f duration:  $186.4 \pm 13.7$  SEM ms, t test,  $p > 0.05$ ). The branch spike prevalence numbers and the dendrite-localized transients reported consisted of recordings from both GCaMP6s and GCaMP6f-expressing dendrites.

To calculate the spatial extent of dendrite localized calcium transients from the high-resolution movies of single dendritic branches *in vivo* and *in vitro* (Figures S3C and S3D), we measured along the length of the dendrite from one edge to the other of the region containing contiguous significant pixels.

### NMDA receptor knockdown

*Grin1<sup>lox/lox</sup>* (B6.129S4-*Grin1<sup>t<sup>m2St</sup></sup>*/J) mice (Tsien et al., 1996) were injected with a high titer Cre -virus (AAV1-CamkII-Cre,  $1.5 \times 10^8$  GC/mL) in combination with a high titer of flexed-GCaMP6 virus (AAV1-Syn-flex-GCaMP6f) leading to expression of GCaMP-6f in a dense CA1 pyramidal neuron population and knockdown of functional NMDA receptors in the same cells expressing GCaMP6f. Imaging of these neurons began ~3 weeks later to ensure sufficient knockdown of NMDA receptors (Chu et al., 2015). For sparse labeling of CA1 pyramidal neurons in *Grin1* mice we replicated the method used to obtain sparse labeling in wild-type mice: a low titer Cre -virus (AAV2/1-CamkII-Cre,  $1.5 \times 10^8$  GC/mL) injected in combination with a high titer of flexed-GCaMP6f virus (AAV1-Syn-flex-GCaMP6f,  $1.4 \times 10^{13}$  GC/mL) leading to sparse expression of GCaMP-6f and knockdown of functional NMDA receptors in the same cells expressing GCaMP6f. We also waited at least 3 weeks before imaging these neurons to ensure NMDA receptor knockdown. The *Grin1* mice required ~1 week more training in F1 to reach behavior criterion (>~2 rewards/minute) compared to wild-type mice.

### NMDA receptor knockdown immunohistochemistry

*Grin1<sup>lox/lox</sup>* mice expressing GCaMP6f and Cre in dorsal hippocampal pyramidal neurons were anaesthetized with isoflurane and perfused with phosphate buffered saline (PBS, pH = 7.4) followed by fixation with 4% paraformaldehyde in PBS. Brains were removed and post-fixed in the same fixative at 4°C overnight, then stored at 4°C in 30% sucrose/PBS solution. Coronal sections (40  $\mu$ m) were prepared using a freezing microtome, washed three times with tris-buffered saline (TBS; pH = 7.6) for 10 minutes

and then incubated with blocking solution (5% normal goat serum, 0.3% Triton X-100 in 1x TBS) for 2 hours at room temperature. The primary antibody (rabbit polyclonal anti-GluN1 IgG, abcam, ab17345; 1:200) was diluted in blocking solution and slices were treated overnight at 4°C. The next day, slices were washed with TBS buffer three times and incubated with diluted secondary antibody (Alexa 594 goat anti-rabbit IgG, 1:500) for 2 hours at room temperature. Slices were washed with TBS buffer three times and then mounted on glass slides in VECTASHIELD (Vector labs, H-1000). Fluorescence images were acquired using an automated slider scanner (VS120 virtual Slide, Olympus).

### Hippocampal slice preparation

Transverse hippocampal slices (~300 µm) were prepared from virus injected male C57BL/6 mice (see Mouse surgery and stereotaxic virus injections) using a vibrating microtome (VT1200S; Leica Systems, Germany). Animals were anaesthetized with isoflurane and perfused with ice-cold sucrose artificial cerebrospinal fluid (ACSF) solution containing (in mM) 85 NaCl, 2.5 KCl, 1.25 NaH<sub>2</sub>PO<sub>4</sub>, 25 NaHCO<sub>3</sub>, 25 glucose, 75 sucrose, 0.5 CaCl<sub>2</sub>, and 4 MgCl<sub>2</sub>, saturated with 95% O<sub>2</sub> and 5% CO<sub>2</sub>. After slices were made they were transferred to a warmed (32°C) incubation chamber with bubbled ACSF consisting of 125 mM NaCl, 2.5 mM KCl, 25 mM NaHCO<sub>3</sub>, 1.25 mM NaH<sub>2</sub>PO<sub>4</sub>, 1 mM MgCl<sub>2</sub>, 2 mM CaCl<sub>2</sub> and 25 mM glucose for 25 min, after which they were allowed to recover at room temperature in oxygenated ACSF for 1 hour before imaging.

### In vitro imaging and glutamate uncaging

Glutamate uncaging and imaging of hippocampal CA1 basal dendrites *in vitro* were performed on an Ultima two-photon laser scanning microscope (Bruker, former Prairie Technologies, Middleton, WI) equipped with duel galvanometers driving two Ti:Sapphire lasers (Chameleon, Coherent). The lasers were tuned to the wavelength of 920 nm and 720 nm for imaging and uncaging, respectively, and the intensity of each laser was independently controlled with electro-optical modulators (Conoptics). Images were acquired with an upright Zeiss Axiovert microscope using a 40x, 1.0 numerical aperture water immersion objective. During imaging and uncaging, slices were maintained at a constant temperature ranging from 30–34°C (mean 32.1°C and bathed in recirculating bubbled ACSF containing 3 mM MNI-caged L glutamate (4-methoxy-7-nitroindolinyl-caged L-glutamate, Tocris), 1 µM TTX (Tocris Bioscience) and 2 µM of GABA<sub>A</sub> receptor antagonist SR-95531 (Tocris Bioscience). MNI-glutamate was uncaged using 500 µs pulses (28-64 mW after the objective) onto varying sequences of 1 to 8 spines with a 120 µs interstimulus interval (all inputs within 5 ms) to evoke local dendritic calcium transients. Uncaging power was adjusted, based on the depth of the dendritic branch, to be in the range of powers previous research has demonstrated generate a post synaptic potential mimicking presynaptic activation with bath applied MNI-glutamate (Bloodgood et al., 2009; Seong et al., 2014). Time-series movies were acquired at ~30 Hz for the duration of uncaging events and were analyzed with MATLAB (MathWorks) and ImageJ following motion correction (see ROI selection and calcium transient analysis). Multiple ROIs were selected for each dendrite by hand and consisted of a ROI encompassing all the pixels with a significant ΔF/F increase at the peak of the transient (Sheffield and Dombeck, 2015) as well as a small ROI drawn on the shaft (~1 um) that was a least 2 spine widths away from the closest uncaging site and another similar sized ROI drawn at the center of each dendritic area of significant ΔF/F increase. These various ROIs were intended to approximate the various sampling cross sections of the dendritic regions that would be expected from the *in vivo* imaging geometry. ΔF/F versus time traces were generated for each ROI as previously described (Dombeck et al., 2010).

## QUANTIFICATION AND STATISTICAL ANALYSIS

Data was analyzed on a Dell Power Edge 720 Server using ImageJ (Version 1.47) and custom software written in MATLAB (Version R2012a and Version R2013b). No statistical methods were used to predetermine sample sizes. Data collection and analysis were not performed blind to the conditions of the experiments. Paired and Unpaired t tests, repeated-measures ANOVA with Tukey's post-test, Bonferroni correction, Wilcoxon rank test and Chi squared test for proportional difference were used to test for statistical significance when appropriate. Statistical parameters including the exact value of n, precision measures (mean ± SEM) and statistical significance are reported in the text and in the figure legends (see individual sections). The significance threshold was placed at p < 0.05.

## DATA AND SOFTWARE AVAILABILITY

Raw data and statistical analysis software can be provided on request. Contact [d-dombeck@northwestern.edu](mailto:d-dombeck@northwestern.edu).